

UNIVERSITY OF SOUTHAMPTON

**The second moment of the
pion's distribution amplitude
from Lattice QCD**

by

Alexandra Jane Dougall

A thesis submitted for the degree of

Doctor of Philosophy

Department of Physics and Astronomy

April 2002

UNIVERSITY OF SOUTHAMPTON

ABSTRACT

FACULTY OF SCIENCE

PHYSICS

Doctor of Philosophy

The second moment of the pion's distribution amplitude
from Lattice QCD

Alexandra Jane Dougall

Two values for the second moment of the pion's distribution amplitude are extracted from a lattice simulation of the appropriate two-point correlation functions. The renormalisation coefficients are calculated by combining the results from one-loop diagrams computed in the lattice regularisation scheme and the $\overline{\text{MS}}$ scheme. A comparison is made with previous lattice studies and QCD sum rule predictions.

I dedicate this thesis to my parents

Contents

Preface	x
Acknowledgements	xi
1 The pion's distribution amplitude	1
1.1 Exclusive processes and form factors	2
1.2 Factorisation in exclusive processes	4
1.2.1 Physical picture	4
1.2.2 Light-cone coordinates	5
1.2.3 Factorisation	7
1.2.4 Comparison with the inclusive case	9
1.3 The distribution amplitude	10
1.3.1 The light-cone expansion	11
1.3.2 The Operator Product Expansion	12

1.3.3	The OPE and its relation to the distribution amplitude	14
1.3.4	Moments	17
1.3.5	The scale dependence of the distribution amplitude	19
1.4	Current status of research	20
1.5	Summary	22
2	Formulating QCD on the lattice	24
2.1	Lattice QCD	25
2.1.1	Euclidean field theory	25
2.1.2	Discretising space-time	27
2.1.3	Gauge fields on the lattice	28
2.1.4	Fermion fields on the lattice	32
2.1.5	Numerical simulations	36
2.1.6	Renormalisation	38
2.2	Errors and sources of uncertainty	39
2.2.1	Statistical errors	39
2.2.2	The quenched approximation	40
2.2.3	Discretisation and $O(a)$ improvement	40
3	The hypercubic group and operator mixing	44

3.1	Operator mixing	44
3.2	Relevant group theory	46
3.2.1	Some basic definitions and properties	46
3.2.2	Representations	47
3.2.3	Reducible and irreducible representations	48
3.2.4	Characters	49
3.3	Decomposition of $O_{\sigma\mu\nu}$ and $O_{\sigma\mu\mu}$ into irreducible representations of \mathcal{H}_4	51
3.3.1	Transformation of $O_{\sigma\mu\nu}$ under \mathcal{H}_4	52
3.3.2	Transformation of $O_{\sigma\mu\mu}$ under \mathcal{H}_4	53
3.4	Summary	54
4	Operator Matching	56
4.1	Matching to the $\overline{\text{MS}}$ scheme	57
4.2	Perturbation theory	58
4.2.1	Continuum perturbation theory	58
4.2.2	Lattice perturbation theory	59
4.3	The matching procedure and associated uncertainties	60
4.4	Results	62
5	Numerical simulation, analysis and results	64

5.1	Lattice computation	64
5.1.1	Simulation details	65
5.1.2	Correlation functions	66
5.2	Analysis and lattice results	68
5.2.1	Correlators and Plateaux	68
5.2.2	Numerical results	71
5.3	Final results and systematic errors	72
5.3.1	Results in the $\overline{\text{MS}}$ scheme	73
5.3.2	Systematic errors	74
6	Conclusions	77
Bibliography		81
A	The moments of a distribution	87
A.1	Expectation	87
A.2	The variance and standard deviation	88
A.3	The moments of a distribution	89
B	Group theory	92
B.1	The hypercubic group	92

B.2	Obtaining the characters for each representation	92
C	Feynman diagrams	98
C.1	Feynman rules	99
C.1.1	Continuum Feynman rules (Minkowski space)	99
C.1.2	Lattice Feynman rules (Euclidean space)	100
C.2	One-loop contributions	101
C.3	An example Feynman diagram on the lattice	103

List of Figures

1.1	$e\pi \rightarrow e\pi$ scattering where the pion-photon interaction is described by the form factor $F_\pi(Q^2)$	3
1.2	Separation of soft and hard physics in electron-pion scattering	5
1.3	Illustration of the light-cone coordinates.	6
1.4	Factorisation of the electromagnetic pion form factor	8
1.5	Hard exchange of gluons contributing to the electromagnetic form factor where (a) $O(\alpha_s)$ contributions (lowest order) and (b) some higher order contributions.	8
1.6	Three- and four-parton distribution amplitudes that are suppressed by factors of $\frac{1}{Q}$. These diagrams are therefore absent in the computation of the form factor at the leading order in Q	9
1.7	Two possibilities for the distribution of momentum between valence quarks where (a) relates to an even distribution (small $\langle \xi^2 \rangle$) [10], and (b) relates to a large fraction of the momentum being carried by one of the valence quarks (large $\langle \xi^2 \rangle$).	19
2.1	The gauge link $U_\mu(x)$ from site x to $x + \mu$	30

2.2	The smallest Wilson loop on the lattice known as a “plaquette”.	31
2.3	The Clover operator that removes $O(a)$ contributions from the Wilson fermion action.	41
3.1	Equivalence between an element of the hypercubic group in four dimensional rotation notation and lattice permutation/reflection notation.	51
5.1	Effective mass plot for $\kappa = 0.13530$. Each fit is an estimate for the energy of the pion (as in Eq. 5.17), and for $\mathbf{p}^2 = 0$, we obtain a value for the mass of the pion.	69
5.2	The fourth component of the axial current plotted on a logarithmic scale at $\mathbf{p}^2 = 1$ and $\mathbf{p}^2 = 2$, for $\kappa = 0.13460$. The straight-line behaviour of each set indicates that the data points fit well to an exponential.	70
5.3	$R_1 (O_{\sigma[\mu\nu]})$ computed in different directions ($p^2 = 2$).	71
5.4	$R_2 (O'_{\sigma\mu\mu})$ computed in different directions ($p^2 = 1$).	72
5.5	$R_1 (O_{\sigma[\mu\nu]})$ and $R_2 (O'_{\sigma\mu\mu})$ with $\kappa = 0.13460$.	73
5.6	The extrapolation of R_1 and R_2 to the zero quark mass limit.	75
6.1	The pion’s distribution amplitude for $\langle \xi^2 \rangle_0 = 1/5$ (asymptotic form), $\langle \xi^2 \rangle_1 = 0.280$ and $\langle \xi^2 \rangle_2 = 0.021$.	78
A.1	Density functions with small and large variance.	90

List of Tables

1.1	Comparison of the factorisation parameters in exclusive amplitudes and inclusive cross sections	10
4.1	One-loop results from the continuum, where $C = \frac{\mu^2}{\lambda^2}$ and $C_F = \frac{4}{3}$	59
4.2	One-loop results from the lattice, where $L = \frac{1}{(a^2 \lambda^2)}$ and $C_F = \frac{4}{3}$	60
4.3	The variation of $\alpha_{\overline{\text{MS}}}(q)$ with scale that will be used in the one-loop matching procedure	62
4.4	Matching coefficients for different α_s with $C_{SW} = 1.0$ and $a\mu = 1.0$	63
5.1	Values of κ shown with the corresponding values of pseudoscalar meson mass [58] (converted into natural units using $a^{-1} = 2.67\text{GeV}$), obtained by fitting to Eq. 5.10.	65
5.2	R_1 and R_2 for different κ	74
6.1	A comparison between the values of $\langle \xi^2 \rangle$ obtained in this study, previous lattice results (all obtained in the lattice regularisation scheme) and QCD sum rules. The errors on $\langle \xi^2 \rangle_{L_{1,2}}$ are statistical only.	80

B.1	Typical element for each conjugacy class of the hypercubic group	93
B.2	Characters of the 24 dimensional representation $O_{\sigma\mu\nu}$	95
B.3	Characters of the 12 dimensional representation $O_{\sigma\mu\mu}$	96
B.4	Characters of the 12 dimensional representation $O_{\sigma\{\mu\nu\}}$ where μ and ν are symmetrised	96
B.5	Characters of the $\mathbf{8}^{(-)}$ dimensional representation	97
B.6	Characters of the $\mathbf{8}^{(+)}$ dimensional representation	97

Preface

Original work appears in Chapters 4 and 5. This was done in collaboration with L. Del Debbio, M. Di Pierro and C.T. Sachrajda, and awaits publication.

Acknowledgements

I would like to begin by thanking my supervisor Chris Sachrajda for his valuable help and guidance throughout this work. I would also like to thank my collaborators, Luigi Del Debbio and Massimo Di Pierro for their input and many useful discussions.

I have enjoyed my time in the SHEP group and the discussions I have had with other members of the group. In particular, I would like to thank David Lin and Sebastien Descotes-Genon for their time and comments regarding the thesis. Thanks also go to John Tighe and Luke Weston for making me feel so welcome when I first arrived in Southampton. In addition, I would like to thank Mike Hill for his computer support.

Thanks to Elspeth and Neil for their encouragement and the pleasant breaks I have spent with them.

Special thanks to Fermin for his companionship and support, this has meant a lot to me.

Most importantly, I would like to acknowledge and thank my parents for their unfailing support and encouragement throughout my studies. I am very grateful to them.

Chapter 1

The pion's distribution amplitude

One of the main achievements of Quantum Field theory is the description of all hadrons through Quantum Chromodynamics (QCD). However, this theory is difficult to handle since its degrees of freedom, quarks and gluons, are not directly observable. This is due to the confining nature of QCD. The strong coupling constant α_s , which is dependent on the energy scale, blows up in the low energy region (≤ 1 GeV), resulting in the confinement of quarks and gluons to form hadrons. In this region, it is therefore impossible to perform perturbative computations through an expansion in powers of α_s . Correspondingly, at high energies QCD exhibits the property of asymptotic freedom i.e., the coupling between quarks and gluons decreases considerably (and vanishes when the scale tends to infinity), thus facilitating computations based on a perturbative expansion. We emphasise however that even at high energies, non-perturbative effects (hadronisation) always have to be considered.

One way to approach this problem is to try to factorise long- and short-distance physics i.e., separate low energies from high energies, the latter of which can be dealt with using perturbative techniques. The hadronisation of quarks and

gluons at low energies is then described by a *distribution amplitude* (or hadronic wavefunction) [1, 2, 3, 4].

In calculating hadronic amplitudes, one must include both the hard perturbative part of the amplitude and the non-perturbative hadronic wavefunctions. Since the exact form of the hadronic distribution amplitudes are still uncertain despite several studies [5, 6, 8, 9, 10, 11, 12, 13, 14], the description of the binding of quarks and gluons to form hadrons is an essential part of the theory that requires more understanding. In this work, we use Lattice QCD (LQCD) to improve on the description of the leading-twist hadronic wavefunction of the pion. Lattice simulations are particularly well suited to this problem since they provide a framework in which to compute Green functions from first principles, with a good control of errors.

In this chapter, we first discuss how factorisation can be applied to exclusive processes at high energies. We then focus on the non-perturbative elements of this approach and in particular, the distribution amplitude. We illustrate how the moments of the pion's distribution amplitude can be related to matrix elements through an operator product expansion, and discuss the significance of the second moment at high energies. Finally, the different approaches to calculating this quantity are reviewed and the present status of the field is discussed.

1.1 Exclusive processes and form factors

There are two different classes of process that can be considered when investigating the strong interactions. The first is high-energy *inclusive* reactions in which only the incoming states are specified. These processes, such as deep inelastic scattering (DIS) however, provide a direct method to investigate the quark content of the hadrons themselves, rather than the way in which the quarks bind

to form hadrons. The strong interactions can also be studied through *exclusive* processes in which the incoming and outgoing states are specified. They can be written in terms of form factors which are Lorentz invariant functions of the momenta of the incoming and outgoing particles. An important source of information is that of electromagnetic form factors, since the photon is a suitable probe with which to examine the structure of the bound state. In such processes, high momentum transfer implies high resolution. Therefore, the hard elastic scattering in $e^- \pi \rightarrow e^- \pi$ provides a natural approach to studying the detailed internal structure of the pion, as illustrated in Fig 1.1.

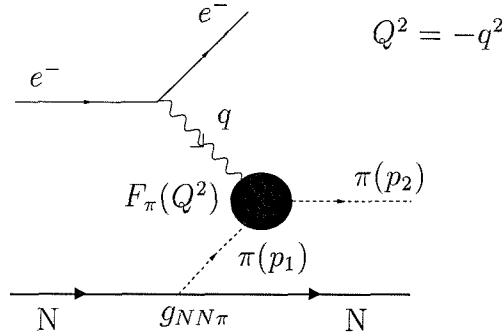


Figure 1.1: $e\pi \rightarrow e\pi$ scattering where the pion-photon interaction is described by the form factor $F_\pi(Q^2)$.

The $\gamma^* \pi\pi$ vertex can be written in terms of the electromagnetic form factor

$$\langle \pi(p_2) | V_\mu(0) | \pi(p_1) \rangle = F_\pi(Q^2)(p_1 + p_2)_\mu \quad (1.1)$$

where $V_\mu(0) = (\frac{2}{3}e\bar{u}\gamma_\mu u - \frac{1}{3}e\bar{d}\gamma_\mu d)$ is the electromagnetic current for the light quarks and $Q^2 = -q^2 > 0$ is the momentum carried by the photon. There is no term proportional to $(p_1 - p_2)_\mu$ due to conservation of the electromagnetic current. The form factor $F_\pi(Q^2)$ is a non-perturbative quantity which contains both the

long-distance effects responsible for the hadronic structure and short-distance interactions between the photon and the constituent partons.

1.2 Factorisation in exclusive processes

In order to isolate the interactions responsible for the hadronic structure of the pion in the exclusive process (Eq. 1.1), long- and short-distances must be separated. We now discuss the physical picture that will enable the factorisation of the form factor $F_\pi(Q^2)$ into hard and soft contributions [10, 15].

1.2.1 Physical picture

The perturbative part of a high-energy process deals with the participating hadrons in their partonic form. For high enough energies, the relative velocities of the participating particles are “light-like”. The binding of the hadron occurs through quantum processes which are highly time dilated in the rest frame of the remaining particles (i.e. the electron for $e^-\pi \rightarrow e^-\pi$). This time dilation results in a lengthening of the lifetime of the states within the hadron and so the partonic content of the pion appears to be “frozen” relative to the electron. As the relative velocities approach the speed of light, the duration for which the particles remain in contact decreases and in this scenario, we expect an absence of quantum interference between the long-distance interactions that ensure the hadronic structure, and short-distance momentum transfers. This incoherence between hard and soft physics suggests that throughout the collision process, the participating hadrons are composed of definite partonic states.

This idea is illustrated by the electron-pion scattering in Fig 1.2, where the soft interactions between the incoming valence quarks are represented by the distri-

bution amplitude ϕ_{in} . The partons in this state then exchange momentum with the electron via a photon, described by the hard-scattering kernel T_H and at a later time, reform into a pion described by the wavefunction ϕ_{out} .

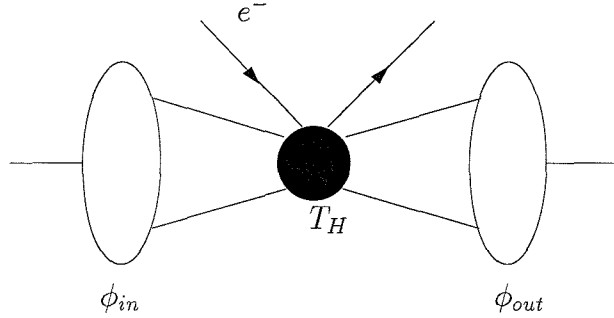


Figure 1.2: Separation of soft and hard physics in electron-pion scattering

1.2.2 Light-cone coordinates

To study the factorisation of high-energy exclusive processes involving light hadrons, it is useful to introduce light-cone coordinates. In $e^-\pi \rightarrow e^-\pi$ for instance, the momenta of the incoming and outgoing pions $p_{in}^2 = p_{out}^2 = m_\pi^2$ are much smaller than the momentum transfer Q^2 . We can therefore make the approximation $p_{in}^2 = p_{out}^2 = 0$, i.e. incoming and outgoing particles are moving on the light-cone. Moreover, the partons that constitute each pion are expected to be collinear to the momentum of the hadron, with only a small transverse momentum. As a first approximation, the momentum of the constituent partons can also be considered as light-like.

A standard four-vector and its modulus squared are defined as

$$v_\mu = (v_0, v_1, v_2, v_3) \quad \text{and} \quad v^2 = v_0^2 - v_1^2 - v_2^2 - v_3^2. \quad (1.2)$$

The light-cone coordinates are then defined as

$$v_{\pm} = \frac{v_0 \pm v_3}{\sqrt{2}} \quad \text{and} \quad \vec{v}_{\perp} = (v_1, v_2), \quad (1.3)$$

such that

$$v_{\mu} = (v_+, v_-, \vec{v}_{\perp}) \quad \text{and} \quad v^2 = 2v_+v_- - \vec{v}_{\perp}^2. \quad (1.4)$$

The two “light-like” vectors $n_+ = (1, 0, \vec{0}_{\perp})$ and $n_- = (0, 1, \vec{0}_{\perp})$ are shown in Fig. 1.3 below

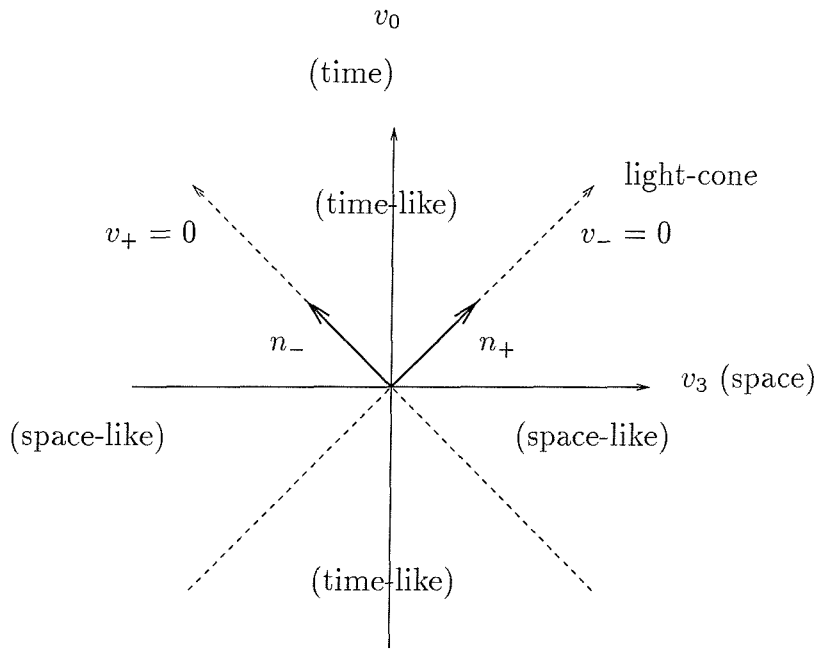


Figure 1.3: Illustration of the light-cone coordinates.

We define the + and - directions for the process of interest ($\pi\gamma^* \rightarrow \pi$):

$$p_{in} = E_{in}n_- \quad (1.5)$$

$$p_{out} = E_{out}n_+ \quad (1.6)$$

1.2.3 Factorisation

We now proceed by factorising the electromagnetic form factor [1, 2, 16]. At very high energies ($Q \rightarrow +\infty$), the exclusive amplitude is dominated by hadronic states with valence quark content ($q\bar{q}$ in the case of the pion). Previous arguments suggest that long- and short-distance effects can be separated, and the corresponding expression for the form factor given in Eq. 1.1, is the convolution

$$F_\pi(q^2) = \int dx dy dz \langle \pi(p_2) | \bar{u}_\alpha^a(x) d_\beta^b(y) | 0 \rangle [T_H(x, y, z, 0)]_{\alpha\beta\gamma\delta}^{abcd} \langle 0 | u_\gamma^c(z) \bar{d}_\delta^d(0) | \pi(p_1) \rangle, \quad (1.7)$$

where higher order corrections are suppressed by factors of $1/Q^2$. Greek and Roman indices denote spin and colour respectively, and the integral is over the spatial coordinates. Since we are outlining the general approach, we do not use light-cone co-ordinates. The perturbative amplitude T_H is computed at the quark level. The bi-local matrix elements represent the hadronisation of quarks and gluons. A path-ordered exponential $\mathcal{P} \exp[\int_0^1 dt z_\mu A_\mu(zt)]$, where A_μ is the gauge field, is inserted in the bi-local matrix elements to maintain gauge invariance¹. This is illustrated in Fig 1.4 where the bi-local matrix elements in Eq. 1.7 that represent the hadronisation of quarks and gluons into a pion are pictured as blobs.

The formula written in Eq. 1.7 is an attempt to factorise soft and hard contributions. In some physical processes, soft gluon exchanges contribute significantly inside the hard scattering kernel. For such cases, soft and hard contributions cannot be disentangled and the factorisation framework breaks down. We therefore note that a consistent factorisation framework requires that soft gluon exchanges must be suppressed in Eq. 1.7.

¹The exponent vanishes in the light-cone gauge and therefore this term is absent in the light-cone formalism.

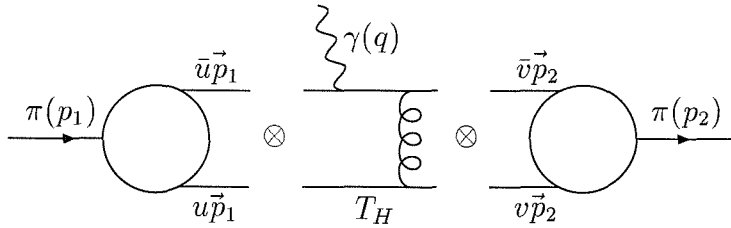


Figure 1.4: Factorisation of the electromagnetic pion form factor

The perturbative kernel T_H describes the hard-scattering of the photon and the partons. At high momentum, since the pion is almost light-like, the valence quarks are approximated to be collinear. Each valence quark of the incoming pion carries a fraction of the total momentum, up_1 or $\bar{u}p_1$ such that $u + \bar{u} = 1$. Correspondingly, the valence quarks of the outgoing pion carry fractions of momentum vp_2 and $\bar{v}p_2$ such that $v + \bar{v} = 1$. Some contributions to T_H are shown in Fig 1.5.

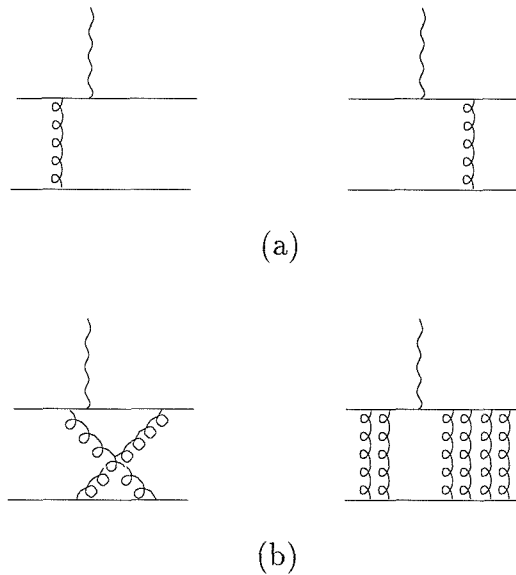


Figure 1.5: Hard exchange of gluons contributing to the electromagnetic form factor where (a) $\mathcal{O}(\alpha_s)$ contributions (lowest order) and (b) some higher order contributions.

Dimensional arguments suggest that distribution amplitudes for three (or more) partons (illustrated in Fig. 1.6) do not contribute to the form factors in the limit $Q \rightarrow \infty$. This has been proved for the process $\pi_0 \rightarrow \gamma\gamma^*$ [2]. The high-energy picture of a pion made up of two valence quarks greatly simplifies the computation of the hard-scattering kernel T_H .



Figure 1.6: Three- and four-parton distribution amplitudes that are suppressed by factors of $\frac{1}{Q}$. These diagrams are therefore absent in the computation of the form factor at the leading order in Q .

Having factorised $F_\pi(Q^2)$ into non-perturbative matrix elements and a perturbative kernel (Eq. 1.7), we can now relate these matrix elements to the pion's distribution amplitude via a light-cone expansion. Before this, we end the section with a brief discussion of factorisation in the inclusive case.

1.2.4 Comparison with the inclusive case

As discussed, the factorisation framework enables the calculation of processes at short-distance or high-momentum transfer. Factorisation can be applied to inclusive as well as hard exclusive processes. In the latter case, the hadronic amplitude is represented by the convolution of a process-dependent hard scattering amplitude T_H (computed at the quark level) with a distribution amplitude ϕ that is process-independent. In the inclusive case ($lp \rightarrow lX$), the cross-section can be expressed as the product of a scale-invariant lepton-quark cross-section $d\sigma$ convoluted with structure functions G . The structure function is a sum of squares of the light-cone distribution amplitudes.

In order to outline the relation between these processes, a comparison of exclusive amplitudes and inclusive cross sections is given in Table 1.1 [4].

exclusive amplitudes	inclusive cross sections
$\mathcal{M} \sim \Pi \phi(x_i, Q) \otimes T_H(x_i, Q)$	$d\sigma \sim \Pi G(x_a, Q) \otimes d\hat{\sigma}(x_a, Q)$
$\phi(x, Q) = \int^Q [d^2 k_\perp] \psi_{val}^Q(x, k_\perp)$	$G(x, Q) = \sum_n \int^Q [d^2 k_\perp] [dx] ' \psi_N^Q(x, k_\perp) ^2$
measure ϕ in $\gamma \rightarrow M \bar{M}$	measure G in $l p \rightarrow l X$
T_H expanded in α_s	$d\hat{\sigma}$ expanded in α_s

Table 1.1: Comparison of the factorisation parameters in exclusive amplitudes and inclusive cross sections

1.3 The distribution amplitude

The motivation underlying the computation of the pion's distribution amplitude exists not only because of the information that it provides on quark binding in hadrons (i.e. the pion). In addition, ϕ_π is an input parameter in several hadronic amplitudes such as the electromagnetic form factor of the pion and $\gamma^* \gamma^* \rightarrow \pi$ which is studied by the CLEO collaboration [17]. The study of B -decays also benefits from a better knowledge of ϕ_π . It has recently been proved that two-body decays, such as $B \rightarrow \pi\pi$ [18, 19], can be computed in the framework of factorisation in the heavy quark limit $m_b \rightarrow \infty$. The analysis of current data from BELLE [20], and BABAR [21] would also benefit from information on the pion's distribution amplitude.

In this section, the bi-local matrix elements appearing in Eq. 1.7 are expanded near the light-cone and re-expressed in terms of the pion's distribution amplitude. We outline the connection between the light-cone expansion and the Operator Product Expansion (OPE).

1.3.1 The light-cone expansion

The outgoing bi-local matrix element in Eq. 1.7 is expanded near the light-cone [2, 10], i.e. $(x - y)^2 \sim 1/Q^2$, such that

$$\langle \pi(p) | \bar{u}_\alpha(x) d_\beta(y) | 0 \rangle = \frac{if_\pi}{4} \int_0^1 du e^{i(\bar{u}p.x + up.y)} (\not{p} \gamma_5)_{\beta\alpha} \phi(u, Q^2) + h.t. \quad (1.8)$$

where $\phi_\pi(u, Q^2)$ is the distribution amplitude of the pion and $f_\pi = 93$ MeV is the pion decay constant. Although a path-ordered exponential has been inserted to preserve gauge invariance, the exponent vanishes due to the choice of gauge (see Footnote 1, page 7). There are several important points to note in Eq. 1.8

- Eq. 1.8 is written with the underlying assumption that transverse momenta up to Q^2 have been integrated into the bi-local matrix elements, whereas transverse momenta larger than Q^2 will be included in the hard-scattering kernel T_H (see Eq. 1.7)
- A renormalisation scale has been introduced in the definition of ϕ . The renormalisation scale dependence of ϕ will then be cancelled by the scale-dependence in T_H to yield renormalisation scale independent form factors.
- u and \bar{u} are the longitudinal fractions of momentum carried by the valence quarks such that $u + \bar{u} = 1$
- $h.t.$ are terms that yield $\frac{1}{Q}$ -suppressed contributions to form factors. They are said to be higher-twist in the light-cone expansion (where twist is defined in Eq. 1.16), and consist of all the possible terms with the same spinorial structure and quantum numbers as the LHS of Eq. 1.8.

Inserting the Dirac matrix $(\gamma_\mu \gamma_5)_{\alpha\beta}$ into Eq. 1.8 and taking the trace, we obtain

$$\langle \pi(p) | \bar{u}(x) (\gamma_\nu \gamma_5) d(y) | 0 \rangle = -if_\pi p_\nu e^{ip.x} \int du e^{iup(y-x)} \phi(u, Q^2), \quad (1.9)$$



where again, the integration over transverse momenta is implicit. This choice of Dirac matrix isolates the lowest twist term containing the pion's wavefunction. When x and y coincide, Eq. 1.9 reduces to the coupling of the pion to the axial current. The distribution is thus normalised

$$\int_0^1 du \phi(u, Q^2) = 1. \quad (1.10)$$

In the isospin limit $m_u = m_d$, the distribution amplitude of the pion is symmetric under the transformation $u \leftrightarrow \bar{u}$, i.e.

$$\phi(\bar{u}, Q^2) = \phi(u, Q^2). \quad (1.11)$$

This property is a consequence of the symmetry of the pion under G -parity (the combination of an isospin rotation with charge conjugation).

1.3.2 The Operator Product Expansion

At small separations, bi-local operators exhibit a divergent behaviour. This divergent behaviour can be expressed as the sum of products of a local operator with a coefficient function (the so-called Wilson coefficient) depending on the separation z . The local operators should have the same quantum numbers as the initial bi-local operator, and the Wilson coefficients exhibit the same divergent behaviour as $z \rightarrow 0$. The OPE for the time-ordered bi-local operator $\bar{u}_\alpha \left(\frac{z}{2} \right) d_\beta \left(\frac{-z}{2} \right)$ is written as [22]:

$$T \left[\bar{\psi}_\alpha \left(\frac{z}{2} \right) \psi_\beta \left(\frac{-z}{2} \right) \right] = \sum_{j, i \geq j} C_j(z^2) z^{\mu_1} \dots z^{\mu_i} \sum_{k=0}^j d_{ijk} \partial_{\mu_{k+1}} \dots \partial_{\mu_i} O_{\mu_0 \dots \mu_k}^{(m)}(0) [\Gamma_{\mu_0}^{(m)}]_{\beta \alpha}, \quad (1.12)$$

where the local operators are of the form

$$O_{\mu_0 \dots \mu_k}^{(m)}(0) = \bar{\psi} \Gamma_{\mu_0}^{(m)} \overset{\leftrightarrow}{D}_{\mu_1} \dots \overset{\leftrightarrow}{D}_{\mu_k} \psi, \quad (1.13)$$

and the covariant derivative is defined as

$$\overset{\leftrightarrow}{D}_\mu = \overset{\leftrightarrow}{\partial}_\mu - ig A_\mu. \quad (1.14)$$

In Eq. 1.12, m takes the values 1, 2 with $\Gamma_\mu^{(1)} = \gamma_\mu$ and $\Gamma_\mu^{(2)} = \gamma_\mu \gamma_5$, and we note that $m = 2$ is the case of interest later. The Lorentz indices are counted by j and $k \leq j$. The local operators defined in Eq. 1.13 are gauge-invariant and traceless, and have the same quantum numbers as the bi-local operator on the LHS of Eq. 1.12.

The Wilson coefficients C_j carry the singularities of the matrix element in the expansion. The short-distance behaviour of these coefficients is obtained by dimensional counting

$$\lim_{z^2 \rightarrow 0} C_j(z^2) = (z^2)^{(d_k^{(m)} - k - D)/2} (\ln(z^2 \mu^2))^\rho, \quad (1.15)$$

where $d_k^{(m)}$ and k are the dimension and spin respectively of the local operators $O_{\mu_0 \dots \mu_k}^{(m)}$, μ is the renormalisation scale, ρ is the anomalous dimension of the local operator and D is the dimension of the bi-local operator. The singularity of the Wilson coefficients is dependent on the twist τ of the operators, defined as

$$\tau = d_k^{(m)} - k \quad (1.16)$$

The leading (most singular) term in Eq. 1.12 corresponds to the operators with

the lowest twist. In the case of the bi-local operator defined in Eq. 1.9, the lowest twist is $\tau = 2$. The corresponding operators are of the form

$$O_{\mu_0} = \bar{\psi} \gamma_{\mu_0} \gamma_5 \psi \quad (1.17)$$

$$O_{\mu_0 \mu_1} = \bar{\psi} \gamma_{\mu_0} \gamma_5 \overset{\leftrightarrow}{D}_{\mu_1} \psi \quad (1.18)$$

$$O_{\mu_0 \mu_1 \mu_2} = \bar{\psi} \gamma_{\mu_0} \gamma_5 \overset{\leftrightarrow}{D}_{\mu_1} \overset{\leftrightarrow}{D}_{\mu_2} \psi \quad (1.19)$$

...

$$O_{\mu_0 \dots \mu_n} = \bar{\psi} \gamma_{\mu_0} \gamma_5 \overset{\leftrightarrow}{D}_{\mu_1} \dots \overset{\leftrightarrow}{D}_{\mu_n} \psi, \quad (1.20)$$

When sandwiched between a pion and the vacuum, O_{μ_0} is related to the pion decay constant and $O_{\mu_0 \mu_1}$ vanishes because the wavefunction is symmetric under G -parity². The first non-trivial matrix element involved at the lowest twist contains the operator

$$\bar{\psi} \gamma_{\mu_0} \gamma_5 \overset{\leftrightarrow}{D}_{\mu_1} \overset{\leftrightarrow}{D}_{\mu_2} \psi. \quad (1.21)$$

This operator is dominant at small z since it has the largest anomalous dimension of all the possible lowest twist operators and therefore (from Eq. 1.15), its Wilson coefficient is the most singular.

1.3.3 The OPE and its relation to the distribution amplitude

We can now make the connection between the OPE in Eq. 1.12 and the moments of the distribution amplitude $\phi_\pi(x, \mu)$ [22]. Using translational invariance, the

²Only even moments of the distribution amplitude are non-vanishing.

light-cone expansion in Eq. 1.9 can be re-written as

$$\left\langle \pi(p) \left| \bar{u} \left(\frac{z}{2} \right) \gamma_\mu \gamma_5 d \left(\frac{-z}{2} \right) \right| 0 \right\rangle = -i f_\pi p_\mu \int_0^1 du e^{i(\bar{u}p\frac{z}{2} - up\frac{z}{2})} \phi(u, Q^2). \quad (1.22)$$

At this stage, we include the renormalisation scale-dependence on Q^2 explicitly.

As discussed in Sec. 1.3.1, Eq. 1.22 is shorthand notation for

$$\begin{aligned} & \int^{Q^2} \frac{d^2 \vec{k}_\perp}{(2\pi)^2} \int d^2 \vec{z}_\perp e^{-i \vec{k}_\perp \cdot \vec{z}_\perp} \left\langle \pi(p) \left| \bar{u} \left(\frac{z}{2} \right) \gamma_\mu \gamma_5 d \left(\frac{-z}{2} \right) \right| 0 \right\rangle \Big|_{z_+ = 0} \\ &= -i f_\pi p_\mu \int_0^1 du e^{\frac{i}{2} p_+ z_- - (\bar{u} - u)} \phi(u, Q^2), \quad (1.23) \end{aligned}$$

We note here that in using light coordinates, $p.z = p_+ z_- + p_- z_+ - \vec{p}_\perp \cdot \vec{z}_\perp$, and that we choose $p_- = 0$ and $p_\perp = 0$ (because p^2 is light-like). A Fourier transformation is used to eliminate the exponent on the RHS of Eq. 1.23 and so we obtain the complete expression for the distribution amplitude

$$\begin{aligned} \phi(u, Q^2) &= \frac{i}{f_\pi} \int \frac{dz_-}{2\pi} e^{-\frac{i}{2} p_+ z_- - (\bar{u} - u)} \int^{Q^2} \frac{d^2 \vec{k}_\perp}{(2\pi)^2} \int d^2 \vec{z}_\perp e^{-i \vec{k}_\perp \cdot \vec{z}_\perp} \\ &\quad \left\langle \pi(p) \left| \bar{u} \left(\frac{z}{2} \right) \gamma_+ \gamma_5 d \left(\frac{-z}{2} \right) \right| 0 \right\rangle \Big|_{z_+ = 0}. \quad (1.24) \end{aligned}$$

In order to relate the distribution amplitude to the OPE, we insert the Dirac matrix $(\gamma_\mu \gamma_5)_{\alpha\beta}$ into Eq. 1.12 and take the trace. The Wilson coefficients are now defined as

$$\tilde{C}_j^+(Q^2) = 4 \int^{Q^2} \frac{d^2 \vec{k}_\perp}{(2\pi)^2} \int d^2 \vec{z}_\perp e^{-i \vec{k}_\perp \cdot \vec{z}_\perp} C_j^+(-z_\perp^2). \quad (1.25)$$

With this definition, we can relate $\phi(u, Q^2)$ directly to the OPE:

$$\phi(u, Q^2) = \frac{i}{f_\pi} \int \frac{dz_-}{(2\pi)} e^{\frac{i}{2} p_+ z_- - (u - \bar{u})} \sum_{j, i \geq j} \tilde{C}_j^+(Q^2) z^{\mu_1} \dots z^{\mu_i}$$

$$\sum_{k=0}^j d_{ijk} \partial_{\mu_{k+1}} \dots \partial_{\mu_i} \langle \pi | \bar{\psi}(0) \gamma_+ \gamma_5 \overset{\leftrightarrow}{D}_{\mu_1} \dots \overset{\leftrightarrow}{D}_{\mu_k} \psi(0) | 0 \rangle, \quad (1.26)$$

$$= \frac{i}{f_\pi} \int \frac{dz_-}{(2\pi)} e^{\frac{i}{2} p_+ z_- (u - \bar{u})} \sum_{j, i \geq j} \sum_{k=0}^j \left[\frac{-i}{2} (u - \bar{u}) \right]^{i-k} (p_+ z_-)^i d_{ijk} b_k \tilde{C}_j^+(Q^2), \quad (1.27)$$

where

$$\langle \pi(p) | \bar{\psi} \gamma_+ \gamma_5 \overset{\leftrightarrow}{D}_{\mu_1} \dots \overset{\leftrightarrow}{D}_{\mu_k} \psi(0) | 0 \rangle = b_k p_+ p_{\mu_1} \dots p_{\mu_k}, \quad (1.28)$$

and integration by parts has been used to convert the external derivatives $\partial_{\mu_{k+1}} \dots \partial_{\mu_i}$ into factors of $\frac{-i}{2} p_+ (u - \bar{u})$. This also produces terms from the derivative acting on the $z^{\mu_1} \dots z^{\mu_i}$ in Eq. 1.27, however these are trace terms which are subtracted. Noting that

$$\int \frac{dz_-}{2\pi} z_-^n e^{\frac{i}{2} p_+ z_- (u - \bar{u})} = \frac{(-2i)^n}{p_+^n} \frac{\partial^n}{\partial(u - \bar{u})^n} \delta(p_+ (u - \bar{u})), \quad (1.29)$$

Eq. 1.27 can now be written in the form

$$\phi(u, Q^2) = \sum_{j, i \geq j} \sum_{k=0}^j \frac{(-1)^{2i-k} (2)^k (i)^{2i-k+1}}{f_\pi} d_{ijk} \tilde{C}_j^+(Q^2) \left[\frac{\partial^i}{\partial(u - \bar{u})^i} \delta(u - \bar{u}) \right] (u - \bar{u})^{i-k} b_k. \quad (1.30)$$

Having obtained an expression which clearly relates the distribution amplitude to the operators appearing in the OPE of Eq. 1.12, we proceed to look at the moments.

1.3.4 Moments

The moments (see A.7 for an introduction to the moments of a distribution) reveal the shape and structure of a distribution. The n^{th} moment of the pion's distribution amplitude is defined as

$$\langle \xi^n \rangle = \int d\xi \xi^n \phi(\xi, Q^2), \quad (1.31)$$

where $\xi = u - \bar{u}$. Relating this to Eq. 1.30, the moments are defined as

$$\begin{aligned} \langle \xi^n \rangle &= \sum_{j,i \geq j} \sum_{k=0}^j \frac{(-1)^{2i-k} (2)^k (i)^{2i-k+1}}{f_\pi} \\ &\quad d_{ijk} \tilde{C}_j^+(Q^2) \int_{-1}^1 d\xi \xi^{n+i-k} \left[\frac{\partial^i}{\partial \xi^i} \delta(\xi) \right] b_k. \end{aligned} \quad (1.32)$$

Using integration by parts,

$$\begin{aligned} &\int_{-1}^1 d\xi \xi^{n+i-k} \left[\frac{\partial^i}{\partial \xi^i} \delta(\xi) \right] \\ &= \int_{-1}^1 d\xi (-1)^i \xi^{n-k} \delta(\xi) (n+i-k) \dots (n-k+1) \\ &= \delta_{kn} (-1)^i i! \end{aligned} \quad (1.33)$$

Since there is a delta function, the above expression vanishes unless $k = n$, and therefore Eq. 1.31 is given by

$$\int_{-1}^1 d\xi \xi^n \phi(u, Q^2) = \frac{i}{f_\pi} \left(\sum_{i,j,n} (-1)^{2i-n} (2)^n (i)^{2i-n} d_{ijn} \right) \tilde{C}_j^+(Q^2) b_n. \quad (1.34)$$

We note here that for the remainder of this subsection, the Wilson coefficients will not be included in the definition of the moments. The following equations are therefore dependent on the renormalisation scheme and scale, and the Wilson coefficients (computed from T_H) must be included in order to obtain a physical

result.

From Eq. 1.34, we see that the n^{th} moment is related to the operators with n derivatives. This is equivalent to inserting operators with derivatives into Eq. 1.8. The first moment is obtained by inserting one derivative to give

$$\langle \pi(p) | \bar{u}(y) \gamma_{\mu_0} \gamma_5 \overset{\leftrightarrow}{D}_{\mu_1} d(y) | 0 \rangle = f_\pi p_{\mu_0} p_{\mu_1} e^{ip \cdot y} \int_0^1 du (u - \bar{u}) \phi(u, Q^2). \quad (1.35)$$

The first moment vanishes since ϕ is symmetric under the interchange of $u \leftrightarrow \bar{u}$. The lowest non-trivial moment of the pion's distribution amplitude is the second moment, which provides information on the momentum distribution between the valence quarks in the pion's wavefunction. For the purpose of this study, we now restrict ourselves to this moment and note that from previous arguments about the twist τ , this will be the most dominant term. Inserting two covariant derivatives into Eq. 1.9, when x and y coincide, we obtain

$$\langle \pi | \bar{u}(y) \gamma_{\mu_0} \gamma_5 \overset{\leftrightarrow}{D}_{\mu_1} \overset{\leftrightarrow}{D}_{\mu_2} d(y) | 0 \rangle = f_\pi p_{\mu_0} p_{\mu_1} p_{\mu_2} \langle \xi^2 \rangle. \quad (1.36)$$

The second moment $\langle \xi^2 \rangle$ enables us to discriminate between different types of distribution amplitude. Two extreme examples are shown in Fig. 1.7, where the distribution in Fig. 1.7(a) corresponds to a small value of $|\langle \xi^2 \rangle - 1/5|$, similar to that of the asymptotic form of the wave function³. For a relatively large value of $|\langle \xi^2 \rangle - 1/5|$, the corresponding distribution is shown in Fig. 1.7(b), which is similar to the form predicted in Ref. [10].

³At very high energy, the wavefunction assumes an asymptotic form, for which $\langle \xi^2 \rangle = 1/5$.

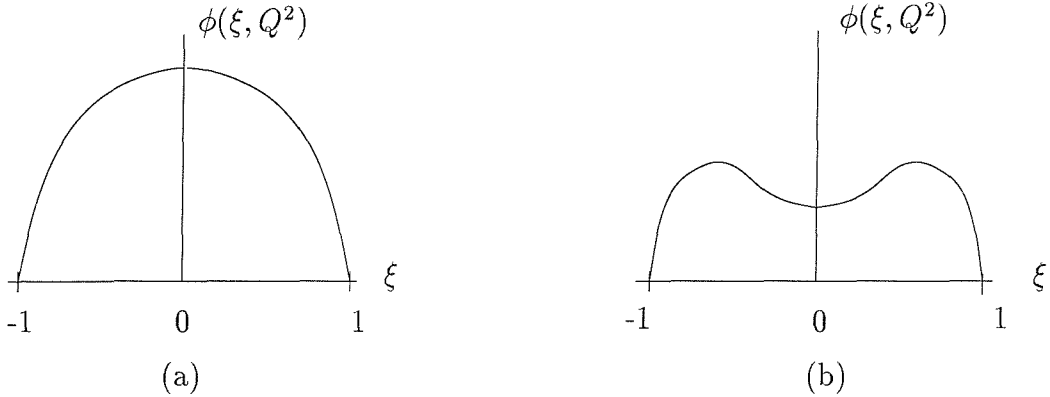


Figure 1.7: Two possibilities for the distribution of momentum between valence quarks where (a) relates to an even distribution (small $\langle \xi^2 \rangle$) [10], and (b) relates to a large fraction of the momentum being carried by one of the valence quarks (large $\langle \xi^2 \rangle$).

1.3.5 The scale dependence of the distribution amplitude

Since the form factor $F_\pi(Q^2)$ is an observable, it must be independent of the renormalisation scale μ , i.e.

$$\mu \frac{d}{d\mu} F_\pi(Q^2) = 0. \quad (1.37)$$

As stated previously, the μ -dependence of the distribution amplitude is cancelled by the μ -dependence in T_H . By increasing the scale μ (at which F_π is factorised), contributions from lines that are off-shell by $O(\mu^2)$ are shifted from T_H to ϕ_π . Thus the derivative of ϕ_π with respect to μ can be calculated in perturbation theory. The evolution of ϕ_π is defined as [2, 3]:

$$\mu \frac{d\phi(u, \mu^2)}{d\mu} = \int_0^1 dz V(u, z, \alpha_s(\mu^2)) \phi_\pi(z, \mu^2), \quad (1.38)$$

where the kernel V is a distribution, known at two-loops [23]. The most general solution to V at the one-loop level is an expansion in Gegenbauer polynomials

$C_n^{\frac{3}{2}}$ [2, 3],

$$\phi_\pi(u, \mu^2) = 6u(1-u) \sum_{n \geq 0} a_n C_n^{\frac{3}{2}} (2u-1) \left(\ln \frac{\mu^2}{\Lambda^2} \right)^{-\frac{\gamma_n}{2\beta_2}}, \quad (1.39)$$

which can be rederived from Eq. 1.30 [22], γ_n are anomalous dimensions related to the operators in Eq. 1.20 ($\gamma_0 = 0$ and $\gamma_{n>0} > 0$), $\beta_2 = (33 - 2n_f)/12$ and the a_n are arbitrary coefficients. The n in Eq. 1.39 must be even because of the symmetry $\phi_\pi(u) = \phi_\pi(\bar{u})$. As $\mu^2 \rightarrow \infty$, Eq. 1.39 reduces to the “asymptotic” form of the wavefunction, given by

$$\phi_0(x) = 6x(1-x). \quad (1.40)$$

As μ^2 decreases, higher order coefficients, i.e. $a_2, a_4 \dots$ become more important in Eq. 1.39. We note that a_2 is related to the second moment of the distribution amplitude.

1.4 Current status of research

There have been several studies concerned with this quantity both on the lattice [5, 6, 7, 8, 9] and using QCD sum rules [10, 11, 24, 25].

The results from QCD sum rules for the second moment are

$$\langle \xi^2 \rangle = 0.4 \pm (15 - 20)\% \quad (\text{at } Q = 1.22 \text{ GeV}) \quad [10, 24], \quad (1.41)$$

$$\langle \xi^2 \rangle = 0.39 \quad (\text{at } Q = 1.5 \text{ GeV}) \quad [11], \quad (1.42)$$

$$\langle \xi^2 \rangle = 0.4 \pm (10 - 15)\% \quad (\text{at } Q = 0.5 \text{ GeV}) \quad [25]. \quad (1.43)$$

These values of $\langle \xi^2 \rangle$ relate to a broad distribution amplitude where the fraction

of momentum shared between valence quarks is unequal. The main idea in the sum rule approach [26], is to equate two representations of a Green function. The first involves condensates through OPE, and the second is a dispersive integral involving the imaginary part of the Green function, which can be related to the moments. The sum rule approach requires a non-perturbative input, namely condensates like $\langle 0|\bar{q}q|0\rangle$, $\langle 0|G_{\mu\nu}G_{\mu\nu}|0\rangle, \dots$, the values of which are still subject to discussion. Moreover, it is necessary to assume that the lowest dimensional condensates are sufficient for a meaningful result.

The operator matrix elements have also been studied previously using lattice techniques. For example, $\langle\xi^2\rangle$ was computed on a $10^3 \times 20$ lattice, with Wilson fermions in the quenched approximation [6, 7]. The result for the second moment is

$$\langle\xi^2\rangle = 0.26 \pm 0.13, \quad (1.44)$$

in the lattice renormalisation scheme at $a \sim (1.8 \text{ GeV})^{-1}$ which is smaller than the sum rules result and implies the distribution illustrated in Fig. 1.7(a). Other lattice predictions for this quantity, all of which were computed in the lattice regularisation scheme, include

$$\langle\xi^2\rangle = 0.235(25) \quad (\text{at } Q = 1.0 \text{ GeV}) [5], \quad (1.45)$$

$$\langle\xi^2\rangle = 0.30(13) \quad (\text{at } Q = 1.9 \text{ GeV}) [8], \quad (1.46)$$

$$\langle\xi^2\rangle = 0.11(2) \quad (\text{at } Q = 2.4 \text{ GeV}) [9], \quad (1.47)$$

$$\langle\xi^2\rangle = 0.10(1) \quad (\text{at } Q = 2.4 \text{ GeV}) [9]. \quad (1.48)$$

Since these results were established, techniques in lattice calculations (such as $O(a)$ improvement) and computing capabilities have been enhanced leading to cleaner signals with smaller errors. With this motivation, it is expedient to re-

calculate this quantity.

1.5 Summary

In this chapter, we began with a discussion of the necessity for a more accurate treatment of non-perturbative effects in QCD. These effects are considered within the context of exclusive processes at high energies (described in terms of form factors), which in certain cases, can be factorised into long- and short-distance contributions [22, 3]. In particular, the electromagnetic form factor describing $e^-\pi \rightarrow e^-\pi$ can be written as the convolution of a hard scattering kernel (computed at the quark level), and matrix elements of fermionic bilinears (Eq. 1.7).

Using a light-cone expansion, the bi-local matrix elements are then written in terms of a Fourier transform of the pion's distribution amplitude ϕ (Eq. 1.24). The bi-local matrix elements themselves exhibit divergent behaviour at short distances and can be expressed (via an OPE) as the sum of products of a local operator with a coefficient function. Having defined the OPE for the fermionic bilinear in Eq. 1.7, the associated local operators are identified, and their relation to the moments of the distribution amplitude is outlined. The n^{th} moment of the distribution ϕ is defined as [24]

$$\langle \xi^n \rangle \equiv \int d\xi \xi^n \phi(\xi, Q^2). \quad (1.49)$$

Its relation to the matrix elements of the local operators appearing in the OPE is given by

$$\langle 0 | O_{\mu_0 \dots \mu_n}(0) | \pi \rangle = f_\pi p_{\mu_0} \dots p_{\mu_n} \langle \xi^n \rangle + \dots \quad (1.50)$$

where

$$O_{\mu_0 \dots \mu_n}(0) = \psi \gamma_{\mu_0} \gamma_5 \overleftrightarrow{D}_{\mu_1} \dots \overleftrightarrow{D}_{\mu_n} \psi \quad (1.51)$$

and the ellipsis indicates terms which can be removed by subtracting traces. This study uses lattice QCD to compute the matrix elements appearing in Eq. 1.50 for $n = 2$.

Chapter 2

Formulating QCD on the lattice

As discussed in Ch. 1, a key feature of the coupling constant g in QCD is that it decreases as the scale at which it is defined increases. This property, known as *asymptotic freedom*, enables the utilisation of perturbation theory in the calculation of short-distance contributions to a process. The quarks and gluons that participate in these hard processes interact at distances of less than 0.1fm. However, the binding of quarks and gluons to form hadrons, known as *confinement*, is a long-distance ($\sim 1\text{fm}$) effect where the magnitude of the coupling constant prohibits the use of a perturbative expansion. In order to calculate physically measurable quantities from QCD, it is therefore essential to use non-perturbative methods such that long-distance effects are dealt with.

We find that providing these long-distance effects can be expressed in terms of matrix elements of local operators (where the external states are single particles or the vacuum)¹, composed of quarks and gluons, it is possible to calculate such amplitudes using the formulation of QCD on the lattice (LQCD). This enables

¹Recent research [27, 28, 29], shows that matrix elements with two-particle external states might be calculable.

the prediction of important quantities such as decay constants, form factors, mixing amplitudes and the subject of this work, distribution amplitudes.

Having motivated the study of QCD on the lattice as an essential tool in dealing with the non-perturbative contributions, we now consider some of the details of its formulation, the extraction of physical quantities from lattice computations and some of the sources of uncertainty that accompany this theory.

2.1 Lattice QCD

The formulation of QCD on the lattice was first introduced by Wilson [30]. There are a number of steps which lead from QCD in continuous Minkowski space-time to Lattice QCD. Following a Wick rotation to Euclidean field theory, the theory must be discretised and the action defined on the lattice. This procedure introduces a cut-off into the theory which is dependent on the lattice spacing “ a ”. Once the theory is in place, we look at how to extract physical results. As will be discussed in Sec. 2.1.5, Monte Carlo methods are used to compute the Path Integral (PI). Amplitudes are then extracted from the correlators and finally the cut-off dependence must be removed. The material included in this section is based on Refs. [31, 32, 33, 34, 35, 36]

2.1.1 Euclidean field theory

In this section, we make the connection between Minkowski and Euclidean field theory. The generating functional in Minkowski space is defined as

$$Z^M = \int D[G] D[\psi] D[\bar{\psi}] e^{iS[G, \psi, \bar{\psi}]}, \quad (2.1)$$

where G are the gauge fields, ψ and $\bar{\psi}$ are the fermion fields and $S[G, \psi, \bar{\psi}]$ is the action. This can be used to calculate Green functions from which physical quantities are extracted. When calculating short-distance physics, this functional integral is expanded in the regime where the coupling constant g is small and so physical quantities are obtained perturbatively. However, as discussed in Ch. 1, this expansion is not valid over all ranges of the coupling.

The exponent in Eq. 2.1 is imaginary and therefore cannot be computed numerically. By expressing the path integral in Euclidean space, it is possible to compute correlation functions from which matrix elements can be extracted.

The connection between four dimensional Minkowski field theory and four dimensional Euclidean field theory is made through an analytic continuation. By performing the Wick rotation,

$$x_0 \rightarrow -ix_4 \quad (2.2)$$

$$p_0 \rightarrow -ip_4, \quad (2.3)$$

where x_0 is the zeroth component of the four vector x_μ . This leads to the Euclidean convention,

$$x_E^2 = \mathbf{x}^2 + x_4^2, \quad (2.4)$$

$$p_E^2 = \mathbf{p}^2 + p_4^2. \quad (2.5)$$

It should be noted that the Lorentz invariant quantity $t^2 - \mathbf{x}^2$ has been replaced by $\mathbf{x}^2 + x_4^2$, the invariant quantity of $O(4)$ which is the symmetry group of Euclidean

field theory². The Euclidean generating functional is then defined as

$$Z^E = \int D[G] D[\psi] D[\bar{\psi}] e^{-S_E[G, \psi, \bar{\psi}]}.$$
 (2.6)

Having obtained the Euclidean form of the generating functional, space-time must be discretised in a finite volume by creating a lattice on which to perform numerical simulations of the path integral.

2.1.2 Discretising space-time

The process of discretisation replaces continuous space-time by a hypercubic lattice L_E , defined as

$$L_E = \left\{ x \in a\mathbb{Z}^4 \left| \frac{x_4}{a} = 0, 1, \dots, T-1; \frac{x_{1,2,3}}{a} = 0, 1, \dots, L-1 \right. \right\},$$
 (2.7)

where a is the lattice spacing³, T is the number of sites in the temporal direction, L is the number of sites in the spatial direction. From this, the number of sites on the lattice is given by $L^3 T$. We note that the volume of the lattice is finite and that the number of degrees of freedom is now finite. Discretisation also demands the replacement of the integrals over space-time by sums, and derivatives with respect to space-time by finite differences⁴.

Having discretised space-time, the momenta can be chosen to lie in the first Brillouin zone $-\frac{\pi}{a} < p \leq \frac{\pi}{a}$. A further consequence of discretisation is the

²See Ch. 3 for further discussion on the reduction in symmetry by formulating QCD on the lattice.

³This work only considers four-dimensional isotropic lattices.

⁴The replacement of derivatives by finite differences will be discussed in section 2.1.3.

introduction of a momentum cut-off

$$\Lambda = \frac{\pi}{a}, \quad (2.8)$$

and so the lattice itself acts as an ultra-violet regulator of QCD⁵.

2.1.3 Gauge fields on the lattice

The continuum QCD action in Euclidean space is given by

$$S_E = - \sum_q \int_x \bar{\psi}_q (\not{D} + m_q) \psi_q + \frac{1}{2} \int_x Tr(F_{\mu\nu} F_{\mu\nu}), \quad (2.9)$$

with the following definitions:

- ψ and $\bar{\psi}$ represent the quark and antiquarks of flavour q
- $\not{D} = \gamma_\mu D_\mu$ where the covariant derivative is defined by

$$D_\mu = \partial_\mu - igA_\mu. \quad (2.10)$$

$A_\mu = A_\mu^a T^a$ are the gauge fields associated with the gluons and T^a are the generators of the colour $SU(3)$ Lie algebra

$$[T^a, T^b] = if^{abc}T^c \quad \text{and} \quad Tr(T^a T^b) = \frac{1}{2}\delta^{ab}. \quad (2.11)$$

- The gauge field strength $F_{\mu\nu}$ is defined as

⁵Regularisation and renormalisation in LQCD will be discussed further in Sec. 2.1.6

$$F_{\mu\nu} = \frac{i}{g} [D_\mu, D_\nu]. \quad (2.12)$$

In the continuum, a gauge transformation on a quark field causes it to pick up a phase factor given by the path ordered product

$$q(x) = L(x, y)q(y), \quad (2.13)$$

where $L(x, y) = \mathcal{P}e^{\int_y^x igA_\mu(z)dz_\mu}$ and the ordering is such that $A_\mu(z)$ is always to the right of $A_\mu(z + dz)$. The gauge transformation of a path ordered exponential depends only on its end points

$$L(x, y) \rightarrow V(x)L(x, y)V^{-1}(y), \quad (2.14)$$

and so the quantity $\bar{q}(x)L(x, y)q(y)$ is gauge invariant. Another gauge invariant product is the trace of the path-ordered integral around any closed path

$$Tr[L(x, x)] \rightarrow Tr[V(x)L(x, x)V^{-1}(x)] \quad (2.15)$$

$$= Tr[L(x, x)], \quad (2.16)$$

known as a Wilson Loop. Since $L(x, y)$ transports the gauge rotation from one point to another, it suggests that on the lattice, the gauge field should be placed on the links connecting the sites, rather than the sites themselves. Following this, we define a discrete analogue of the path ordered product

$$U_\mu(x) = e^{iagA_\mu(x + \frac{a\mu}{2})}, \quad (2.17)$$

as shown in Fig. 2.1 below. $U_\mu(x)$ is an element of $SU(3)$ associated with the link from site x to site $x + a\mu$.

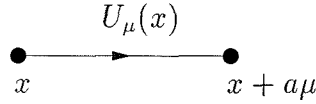


Figure 2.1: The gauge link $U_\mu(x)$ from site x to $x + \mu$.

In the continuum limit, this corresponds to a line integral along the link, i.e.

$$U_\mu(x) \sim L(x, x + a\mu) \quad (2.18)$$

$$= 1 - i a g A_\mu(x + \frac{a\mu}{2}) + O(a^2). \quad (2.19)$$

The gauge transformations of the U fields are

$$U_\mu(x) \rightarrow V(x) U_\mu(x) V^\dagger(x + a\mu), \quad (2.20)$$

where $V(x) \in SU(3)$ are the gauge transformation matrices that sit on the sites. From Eq. 2.20, it can be seen that the trace of a closed product of U 's in a closed loop will be invariant under gauge transformations (since $V(x)V^\dagger(x) = 1$) and from this, we can define a Wilson loop on the lattice.

We now construct the lattice analogue of the pure gauge action by constructing the smallest Wilson loop on the lattice

$$P_{\mu\nu} = U_\mu(x) U_\nu(x + a\mu) U_\mu^\dagger(x + a\nu) U_\nu^\dagger(x), \quad (2.21)$$

known as a plaquette and shown below in Fig. 2.2.

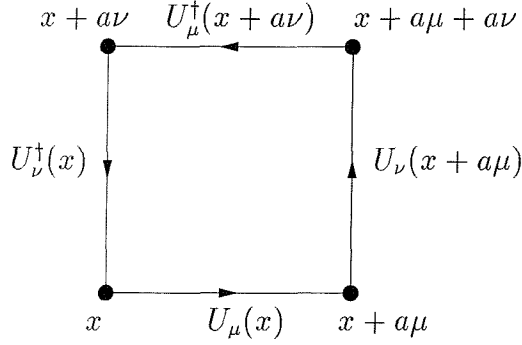


Figure 2.2: The smallest Wilson loop on the lattice known as a “plaquette”.

By inserting the definition of the link variable (Eq. 2.17) into Eq.2.21 and using the Baker-Campbell-Hausdorff relation,

$$e^A e^B = e^{A+B+\frac{1}{2}[A,B]+\dots}, \quad (2.22)$$

we find that Eq. 2.21 reduces to

$$P_{μν} = 1 + \frac{ia g^2}{2} λ^a F_{μν}^a - \frac{a^4 g^2}{4} λ^a λ^b F_{μν}^a F_{μν}^b + ia^3 G_{μν} + ia^4 H_{μν} + O(a^5). \quad (2.23)$$

Taking the trace of Eq. 2.23 and keeping only Real parts gives

$$\mathbb{R}[Tr(P_{μν})] = N_c - \frac{a^4 g^2}{2} Tr(F_{μν}^2) + O(a^6), \quad (2.24)$$

where N_c is the number of colours. From this, we obtain the relation between the continuum and the lattice pure gauge action:

$$\int d^4x \sum_{μν} \frac{1}{2} Tr[F_{μν} F_{μν}] \sim \sum_{μν} \frac{2}{g^2} (N_c - \mathbb{R}[Tr(P_{μν})]) + O(a^2), \quad (2.25)$$

where N_c is the number of colours. Finally, re-writing $\beta = \frac{2N_c}{g^2}$, we define the Wilson gauge action

$$S_g^W = -\beta \sum_{\mu\nu} \frac{\mathbb{R}[Tr P_{\mu\nu}]}{N_c}. \quad (2.26)$$

Before constructing the functional integral from Eq. 2.26, the measure (over the gauge degrees of freedom) must be defined. Since gauge fields are defined on the lattice by the link variables which are $SU(3)$ matrices, the measure must be invariant under group transformations. Following this constraint, the Haar measure is defined as

$$\int dU f(U) = \int dU f(UV) = \int dU f(WU), \quad (2.27)$$

where U and W are elements of the colour $SU(3)$ gauge group. The Haar measure can be normalised as $\int dU = 1$. The functional integral is now written as

$$Z_g = \int \prod_{\text{links}} dU_\mu(x) e^{\beta \sum_{\mu\nu} \mathbb{R}[Tr(P_{\mu\nu})]}. \quad (2.28)$$

2.1.4 Fermion fields on the lattice

From the action in Euclidean space (Eq. 2.9), the fermionic part is described by the term

$$S_q = \bar{\psi}_q (\not{D} + m_q) \psi_q, \quad (2.29)$$

where there is a sum over quark flavour q and the fermion fields ψ_q and $\bar{\psi}_q$ are in the fundamental representation of colour $SU(3)$. In order to discretise this term, the fermion fields are placed on the sites with the following gauge transformation

properties

$$\psi(x) \rightarrow V(x)\psi(x), \quad (2.30)$$

$$\bar{\psi}(x) \rightarrow \bar{\psi}V^\dagger(x). \quad (2.31)$$

The next step is to discretise the derivative. The fermion fields must be separated and link variables are used to maintain gauge invariance. The covariant derivative in Eq. 2.29 is then defined as

$$\bar{\psi}D_\mu\psi(x) = \frac{1}{2a}\bar{\psi}(x)[U_\mu(x)\psi(x+a\mu) - U_\mu^\dagger(x-a\mu)\psi(x-a\mu)]. \quad (2.32)$$

Taylor expanding the fields and dropping higher order terms in a , Eq. 2.32 reduces to the continuum covariant derivative.

$$\bar{\psi}D_\mu\psi = \bar{\psi}[\partial_\mu - igA_\mu]\psi. \quad (2.33)$$

Including the mass term and the γ matrices, we obtain the naive fermion action

$$\begin{aligned} S_q^N(\psi, \bar{\psi}, U) = & \sum_{x,\mu} \frac{1}{2a} \bar{\psi}(x) \gamma_\mu [U_\mu(x)\psi(x+a\mu) - U_\mu^\dagger(x-a\mu)\psi(x-a\mu)] \quad (2.34) \\ & + \sum_x m\bar{\psi}(x)\psi(x). \end{aligned}$$

This can be re-written as

$$S_q^N(\psi, \bar{\psi}, U) = \sum_x \bar{\psi}(x) M_{xy}[U]\psi(y), \quad (2.35)$$

where M is given by

$$M_{x,y}[U] = m_q \delta_{xy} + \frac{1}{2a} \sum_\mu [\gamma_\mu U_{x,y} \delta_{x,y-\mu} - \gamma_\mu U_{x-\mu,\mu}^\dagger \delta_{x,y+\mu}] \quad (2.36)$$

and x and y label the lattice sites and with spin and colour indices suppressed.

Before constructing the complete partition function with Eqs.(2.28,2.35), we note that the naive fermion action in Eq. 2.35 gives rise to a problem known as “fermion doubling” which must be dealt with. The action yields $2^4 = 16$ degenerate states rather than one. To demonstrate how this happens, consider the momentum space free propagator⁶

$$G(k) = \frac{-i\gamma + am_q}{s^2 - (am_q)^2}, \quad (2.37)$$

where $s_\mu = \sin(ap_\mu)$. If we define the momentum range in the Brillouin zone to be $[\frac{-\pi}{2a}, \frac{3\pi}{2a}]$, then in the limit $m_q \rightarrow 0$, we see that for each momenta $ap_\mu = 0$ and $ap_\mu = \pi$, this term will vanish. There is a pole near each of the sixteen possible positions, hence the single lattice fermion represents sixteen degenerate states.

On the lattice, for a pole in the propagator associated with a left-hand (right-hand) field at $ap_\mu = 0$, we actually find a replica of a right-handed (left-handed) field associated to a pole at $ap_\mu = \pi$. In fact, the problem of fermion doubling is strongly related to chiral symmetry on the lattice, as stated by the Neilsen-Ninomiya no-go theorem [37, 38], which states that a fermionic theory on the lattice cannot simultaneously contain the following properties:

- locality (nearest neighbour interaction)
- translational invariance
- Hermiticity
- exact chiral symmetry

⁶This is obtained by setting the gauge links $U_\mu(x) = 1$ and taking the Fourier transform of the inverse Dirac operator in Eq. 2.35.

- no fermion doubling.

Wilson [30] proposed a solution to the problem of fermion doubling by adding an irrelevant operator to the action that explicitly breaks chiral symmetry

$$S_q = \sum_{x,\mu} \frac{r}{2} \bar{\psi}(x) [U_\mu^\dagger(x - \mu) \psi(x - \mu) - U_\mu(x) \psi(x + \mu) - 2\bar{\psi}(x) \psi(x)] \quad (2.38)$$

where r is known as the Wilson parameter. The form of the free propagator originally given in Eq. 2.37 is now modified to

$$G(k) = \frac{-i\cancel{s} + (am_q - \frac{r}{2}\hat{k}^2)}{s^2 - (am_q + \frac{r}{2}\hat{k}^2)^2}, \quad (2.39)$$

where $\hat{k} = 2\sin(\frac{ak_\mu}{2})$. The relation between the mass in the continuum (m_{phys}) and the lattice (m_q) is $am_{phys} = am + \frac{r}{2}\hat{k}^2$. In the case where $ak_\mu = \pi$, we find that $\hat{k} \neq 0$ and so the additional pole (at $ak_\mu = \pi$) gains an effective mass. In the limit $a \rightarrow 0$, with r kept finite, m_{phys} will tend to infinity and the doublers will decouple from the theory. Since chiral symmetry is explicitly broken on the lattice, there is nothing to prevent the quark mass from being additively renormalised. Moreover, the additive renormalisation receives a large correction at the one-loop level [39] and therefore has to be determined non-perturbatively. It is important to note that exact chiral symmetry can be obtained on the lattice using fermions that satisfy the Ginsparg-Wilson relations [40]. However, strict locality is lost [41] due to interactions between fermions that are beyond nearest neighbour (further than the surrounding sites), and this formulation of fermions on the lattice is computationally expensive.

The Wilson action is therefore defined as

$$S_F^W = \sum_{x,y} \bar{\psi}^L(x) M_{xy}^W \psi_y^L, \quad (2.40)$$

where $\psi^L = \sqrt{m_q a + 4r} \psi$ and the interaction matrix $M_{x,y}^W$ is written as

$$M_{x,y}^W[U]a = \delta_{xy} - \kappa \sum_{\mu} [(r - \gamma_{\mu}) U_{x,y-\mu} + (r + \gamma_{\mu}) U_{x-\mu,y+\mu}^{\dagger}] \quad (2.41)$$

with $\kappa = \frac{1}{2am_q + 8r}$, known as the hopping parameter. Together with Eq. 2.26, we define the full Wilson action (including the pure gauge term) as

$$S_W = \sum_{x,y} \bar{\psi}^L(x) M_{xy}^W \psi_y^L - \beta \sum_{\mu\nu} \frac{\mathbb{R}[Tr P_{\mu\nu}]}{N_c}. \quad (2.42)$$

The relation between the fermion action and the continuum is $S_{cont}^F = S_W^F + O(a)$. It therefore will not be the final action that we actually use in this work since the $O(a)$ errors can be removed by Symanzik's "improvement program". This will be discussed further in Sec. 2.2.3.

2.1.5 Numerical simulations

LQCD evaluates matrix elements by computing the PI non-perturbatively as opposed to formulating an asymptotic expansion in the coupling. In this section, we give a brief outline of how these computations are performed. The simulation details particular to this study will be discussed in Ch. 5.

In order to compute the PI, it must be reduced to a finite number of degrees of freedom. This reduction is achieved by introducing a lattice of finite extent in Euclidean space and time.

To demonstrate the major steps involved in simulations we consider the pion two-point function

$$\langle 0 | \Phi(x) \Phi^\dagger(0) | 0 \rangle = Z^{-1} \int [dU] \prod_q [dq] [d\bar{q}] e^{-S_g - S_N - S_W} \bar{u} \gamma_5 d(x) \bar{d} \gamma_5 u(0), \quad (2.43)$$

where $\Phi(x) = \bar{u} \gamma_5 d(x)$ is an interpolating operator for the pion and S_g and $S_N + S_W$ are defined in Eqs.(2.26,2.40),. Eq. 2.43 can be re-written as

$$\frac{- \int [dU] \prod_q \det(\mathcal{D} + m_q) e^{-S_g} \text{Tr} [(\mathcal{D} + m_d)_{x0}^{-1} \gamma_5 (\mathcal{D} + m_u)_{0x}^{-1} \gamma_5]}{- \int [dU] \prod_q \det(\mathcal{D} + m_q) e^{-S_g}}. \quad (2.44)$$

where x and y are lattice sites and $(\mathcal{D} + m_q)$ is the complete lattice Dirac operator appearing in the sum $S_N + S_W$. The second line (Eq. 2.44) is obtained by integrating over the fermion fields leaving a functional integral over gauge fields only, with the measure

$$d\mu = [dU] \prod_q \det(\mathcal{D} + m_q) e^{-S_g}. \quad (2.45)$$

In this study, we work in the quenched approximation which sets the determinant of the fermion matrix to a constant. This approximation and its consequences will be discussed further in Sec. 2.2.2.

A set of gauge configurations is generated with probability measure $d\mu$ using Monte Carlo methods. Propagators $(\mathcal{D} + m_q)^{-1}$ are then computed on each configuration by inverting the matrix given in Eq. 2.41 and joining together into traces as in Eq. 2.44.

In order to extract physical information from the correlator in Eq. 2.43, a complete set of states is inserted and a Fourier transform in the spatial directions is performed. At large time separations, the correlator reduces to

$$\sum_{\vec{x}} e^{-i\vec{p} \cdot \vec{x}} \langle 0 | \Phi(x) \Phi^\dagger(0) | 0 \rangle \stackrel{t \rightarrow \infty}{\equiv} \frac{Z}{2E} e^{-Et}, \quad (2.46)$$

where Z is the pion wavefunction renormalisation constant and E is the energy of the pion. By plotting the log of the correlator at zero momentum, we can extract the mass of the pion on the lattice (am_π).

2.1.6 Renormalisation

The relation between bare and renormalised quantities in QCD can be expressed in terms of a perturbative expansion in the coupling. Any quantity computed on the lattice is defined in terms of the cut-off a . Therefore we need to relate the bare lattice operators to a continuum renormalisation scheme, at a renormalisation scale μ (in this case, $\overline{\text{MS}}$). This procedure is known as “matching”. In Eq. 2.47 below, the bare lattice operator $Q(a)$ is related with $Q(\mu)$ (the operator computed in the $\overline{\text{MS}}$ scheme) by $Z(a\mu)$ (computed through matching)

$$Q(\mu) \sim Z(a\mu)Q(a). \quad (2.47)$$

Physical quantities do not depend on the renormalisation scheme or the scale. Once the lattice operators have been matched to the continuum ones, a physical result A_{phys} is obtained by combining matrix elements in the $\overline{\text{MS}}$ scheme with the Wilson coefficients $C(\mu)$ (computed in the same scheme),

$$A_{phys} \sim C(\mu)Q(\mu). \quad (2.48)$$

The result here is independent of the scheme and scale up to the order that the Wilson coefficient is calculated.

This topic will be discussed in more detail in Ch. 4, where we calculate the relevant Feynman diagrams in both the lattice and continuum schemes, perform the matching procedure and then combine the results with the Wilson coefficients relevant for the operators of interest in this work.

2.2 Errors and sources of uncertainty

There are several sources of uncertainty in lattice calculations. We consider the statistical error, the error due to quenching and the effects of discretisation and $O(a)$ improvement.

2.2.1 Statistical errors

There is an inherent statistical error associated with all quantities computed on the lattice whose origins lie in the finite number of gauge configurations used to compute the PI. It is assumed that the gauge configurations are distributed according to the weight $\exp^{-S[U]}$ (in the quenched approximation), and that the configurations generated are a finite sample of this distribution. The bootstrap procedure [42] is used to estimate the error associated with this sampling.

The bootstrap procedure randomly samples a new set of configurations from the original (allowing repeated resampling of the same configurations) and recalculates the results. This process is repeated “N” times and provides a distribution for each quantity. By looking at the distribution of the bootstrap samples of a quantity, we obtain an estimate of the statistical error associated with it.

2.2.2 The quenched approximation

As stated previously, in the quenched approximation the fermion determinant is set to a constant. This is referred to as Quenched QCD (QQCD). Physically, this constitutes the omission of internal fermion loops and so the vacuum polarisation effects of quark loops are ignored. The motivation for this approximation is the reduction in CPU time. One of the problems with QQCD is that since the internal quark loops (which are necessary to obtain on-shell intermediate states) are absent, resonances become stable states. For many quantities computed on the lattice, the discrepancy between the quenched calculations and that of the physical quantities is about 10%. It is important to note however that the non-perturbative features of QCD are retained in this approximation since QQCD maintains both confinement and chiral symmetry breaking.

2.2.3 Discretisation and $O(a)$ improvement

As stated previously, the action given in Eq. 2.42 contains $O(a)$ errors originating from the fermionic action and $O(a^2)$ terms coming from the pure gauge action. In order to obtain a level of precision at least to $O(a^2)$, it is possible to remove the $O(a)$ contributions by implementing an improvement program.

Improvement of the fermionic action was first outlined by Symanzik [43]. The removal of $O(a)$ contributions was then implemented by Sheikholeslami and Wohlert [44], by defining an additional operator in the action, known as the “Clover” term⁷. The operator is constructed from the sum of four plaquettes in the (μ, ν) plane, stemming from the point x , such that

⁷The action including this term is referred to as the Sheikholeslami-Wohlert action.

$$F_{\mu\nu}^c(x) = \frac{1}{4} \sum_{U=1}^4 \frac{1}{2ig_0a^2} [U_{\mu\nu}(x) - U_{\mu\nu}^\dagger(x)], \quad (2.49)$$

which is represented diagrammatically in Fig. 2.3 and where

$$\begin{aligned} U_{\mu\nu} = & \frac{1}{4} (U_\mu(x)U_\nu(x+a\mu)U_\mu^\dagger(x+\nu)U_\nu^\dagger(x) \\ & - U_\mu^\dagger(x-a\mu)U_\nu^\dagger(x-a\mu-a\nu)U_\mu(x-a\mu-a\nu)U_\nu(x-a\nu) \\ & + U_\nu(x)U_\mu^\dagger(x-a\mu+a\nu)U_\nu^\dagger(x-a\mu)U_\mu(x-a\mu) \\ & - U_\nu^\dagger(x-a\nu)U_\mu(x-a\nu)U_\nu(x-a\mu)U_\mu^\dagger(x)). \end{aligned} \quad (2.50)$$

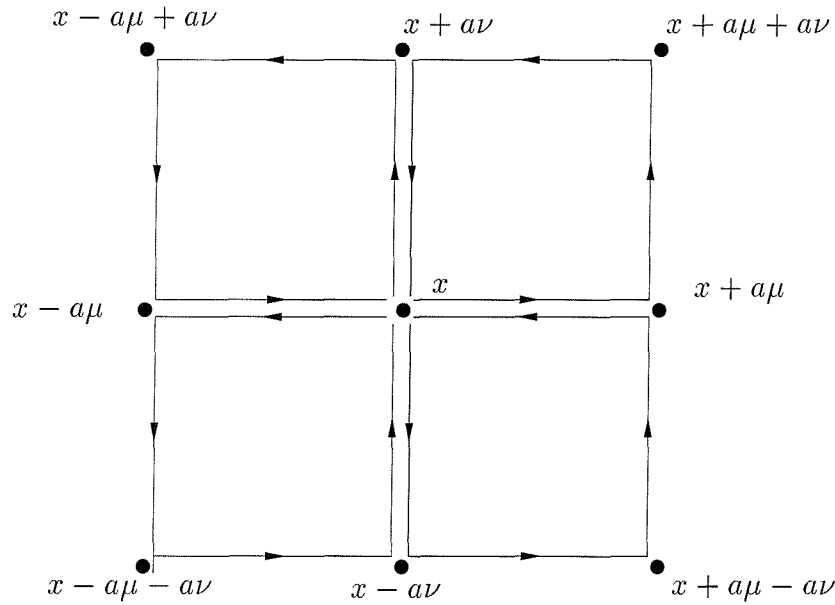


Figure 2.3: The Clover operator that removes $O(a)$ contributions from the Wilson fermion action.

Eq. 2.49 is added to the Wilson fermion action with the coefficient c_{SW}

$$S_{SW} = S_W + a^4 c_{SW} \kappa r \sum_x \bar{\psi} P(x) \psi(x), \quad (2.51)$$

where $P(x) = \frac{ia}{2} \sum_{\mu,\nu} F_{\mu\nu}^c(x) \sigma_{\mu\nu}$ and $\sigma_{\mu\nu} = \frac{-i}{2} [\gamma_\mu, \gamma_\nu]$. In addition to the inclusion of this operator, the fermion fields (in on-shell hadronic matrix elements) undergo the rotation [45]:

$$\begin{aligned} \psi &\rightarrow \psi' = (1 - a \frac{r}{2} \not{D}) \psi + O(a^2) \\ \bar{\psi} &\rightarrow \bar{\psi}' = (1 - a \frac{r}{2} \not{D}) \bar{\psi} + O(a^2). \end{aligned} \quad (2.52)$$

The removal of $O(a)$ errors through the addition of the clover term and the rotation of the fermion fields in the operators reduces the difference between continuum and lattice matrix elements to terms of $O(a\alpha_s)$. These errors can be removed using perturbation theory, where c_{SW} is computed to one-loop. The remaining lowest order errors will then be of $O(a\alpha_s^2)$. By tuning c_{SW} non-perturbatively [46], it is possible to remove all $O(a\alpha_s^n)$ terms in the action. Nevertheless, the procedure of removing such terms from hadronic matrix elements is more involved and this is left to future work.

We finish by stating the exact form of the action (Eq. 2.51) that is used in this study

$$S_{SW} = \sum_{x,y} \bar{\psi}^L(x) M_{xy}^W \psi_y^L - \beta \sum_{\mu\nu} \frac{\mathbb{R}[Tr P_{\mu\nu}]}{N_c} + a^4 c_{SW} \kappa r \sum_x \bar{\psi} P(x) \psi(x), \quad (2.53)$$

where the error in the action due to discretisation is now of $O(a^2)$.

Chapter 3

The hypercubic group and operator mixing

In this chapter, we consider the consequences of the reduction in symmetry due to the replacement of the Lorentz group by the hypercubic group. In particular, we investigate the fact that the reduced symmetry admits greater opportunity for operator mixing and is therefore a major problem which must be dealt with in order to obtain a physical result from the lattice.

3.1 Operator mixing

As established in Ch. 1, in order to calculate moments of the pion's distribution amplitude, we are required to study the matrix elements of the lowest twist local operators between the pion and the vacuum [22].

In the continuum, these operators are classified according to their behaviour under Lorentz transformations and charge conjugation. The leading twist ($\tau =$

2) operators are totally symmetric, traceless tensors and as a result of their transformation properties, do not mix with operators of lower dimension under renormalisation.

A major consequence of modelling QCD on the lattice is the reduction in the spacetime symmetries of the theory. Analytically continuing from Minkowski to Euclidean space replaces the Lorentz group by the orthogonal group $O(4)$. There is a further reduction in symmetry due to the discretisation of spacetime: $O(4) \rightarrow \mathcal{H}_4 \subset O(4)$, and therefore the hypercubic group (\mathcal{H}_4) describes the spacetime symmetries of the lattice.

The opportunity for operator mixing under renormalisation is increased due to the fact that the hypercubic group \mathcal{H}_4 (defined in Sec. 3.3), is a finite group and therefore the symmetries imposed by this group are less restrictive than those of the Lorentz group. Mixing with operators of lower dimension is of concern because the mixing coefficient will contain negative powers of the lattice spacing a . In the limit $a \rightarrow 0$, this will produce power divergences which render the result unphysical [6].

When calculating matrix elements on the lattice, operators must therefore be classified according to their behaviour under \mathcal{H}_4 rather than the Lorentz group and chosen in such a way that for symmetry reasons they cannot mix with lower dimensional operators, thus ensuring the absence of power divergences.

We therefore proceed by searching for a choice of Lorentz indices such that the operators $O_{\mu_0\mu_1\mu_2} = \bar{\psi} \gamma_{\mu_0} \gamma_5 \overset{\leftrightarrow}{D}_{\mu_1} \overset{\leftrightarrow}{D}_{\mu_2} \psi$ satisfy the specified criteria. We could begin by considering the operators $O_{\mu\mu\mu}$. However, operators with this Lorentz structure (all three indices equal) transform like the $(\frac{1}{2}, \frac{1}{2})$ irreducible representation of the hypercubic group and mix under renormalisation with other four dimensional operators, an extensive study of which can be found in Ref. [47].

This leaves the possibility of $O_{\sigma\mu\nu}$ with all three Lorentz indices different and also $O_{\sigma\mu\mu}$ with $\sigma \neq \mu$. In this chapter we investigate the transformation properties of these operators with respect to the hypercubic group.

3.2 Relevant group theory

In this section, we briefly review the group theory necessary to establish the correct Lorentz structure for the operators. The material presented within this subsection is based on Refs. [48, 49].

3.2.1 Some basic definitions and properties

A group G is defined as a set of elements g_1, g_2, g_3, \dots with a rule for combining them called a group multiplication which satisfies the following axioms:

- (i) Closure: the product $g_i g_j$ is also an element in G ;
- (ii) Associativity: the group multiplication is associative

i.e. $(g_i g_j) g_k = g_i (g_j g_k)$;

- (iii) Identity: there exists an element e in G , called the identity, such that

$$eg = ge = g \text{ for all } g;$$

- (iv) Inverse: for each g there is an element g^{-1} such that

$$g^{-1}g = gg^{-1} = e.$$

If the number of elements in G is finite, the group is said to be finite. The order of the group, denoted by $|G|$, is the number of elements within the group and the order of each element g is the least integer n such that $g^n = e$.

Two elements g_1 and g_2 of a group G are said to be in the same conjugacy class C if there is an element g in G such that

$$g_2 = gg_1g^{-1}. \quad (3.1)$$

Any group can be partitioned into classes where each element is in exactly one class only. Elements that are in the same class share the same structural property of the group, that is, they are (geometrically) of a similar kind. We note that each element of a conjugacy class has the same order.

3.2.2 Representations

For our purposes, we are interested in the action of \mathcal{H}_4 on vector spaces, where the basis will be the operators of interest and the action of any element in \mathcal{H}_4 is represented by a matrix.

Consider a set of $n \times n$ non-singular matrices \mathbf{D} corresponding to elements of a finite group G , i.e. $g \rightarrow \mathbf{D}(g) \forall g \in G$, such that the following conditions are satisfied:

$$\mathbf{D}(g_1)\mathbf{D}(g_2) = \mathbf{D}(g_1g_2), \quad (3.2)$$

$$\mathbf{D}(\mathbf{I}) = I. \quad (3.3)$$

The matrix to which the group element g maps is written $\mathbf{D}(g)$ and a complete set of matrices, one for each element of the group, is called an n -dimensional

representation of the group.

3.2.3 Reducible and irreducible representations

Let $\mathbf{D}^{(1)}$ and $\mathbf{D}^{(2)}$ be representations of a group G , with dimensions n_1 and n_2 respectively. Then for each g in G , the assignment

$$\mathbf{D}(g) = \mathbf{D}^{(1)}(g) \oplus \mathbf{D}^{(2)}(g) \quad (3.4)$$

determines a new representation of dimension $n_1 + n_2$, which is called the direct sum of $\mathbf{D}^{(1)}$ and $\mathbf{D}^{(2)}$. A representation is said to be reducible if it is equivalent to a direct sum of the form shown in Eq. 3.4¹. A representation which is not reducible is said to be irreducible and is denoted by $d^{(i)}(g)$. Irreducible representations form the building blocks of representation theory and any (reducible) representation can be written as a direct sum over all possible irreducible representations:

$$\mathbf{D}(g) = m_1 d^{(1)}(g) \oplus m_2 d^{(2)}(g) \oplus \dots \oplus m_N d^{(N)}(g), \quad (3.5)$$

where the integers (m_k) indicate the number of times each particular irreducible representation $d^{(k)}$ is repeated.

We now state the fundamental orthogonality relation for the matrices of irre-

¹A similarity transform (see Eq. 3.7) is usually required in order to obtain the block diagonal form of $\mathbf{D}(g)$.

ducible representations. A proof of this theorem can be found in group theory textbooks, e.g. in Ref. [48]. Let G be a finite group with $|G|$ elements and let $d^{(1)}, d^{(2)}, \dots, d^{(N)}$ be the inequivalent irreducible representations of G , with dimensions n_1, n_2, \dots, n_N respectively. Then

$$\sum_g d_{ij}^{(\alpha)}(g)^* d_{kl}^{(\beta)}(g) = \frac{|G|}{n_\alpha} \delta_{ik} \delta_{jl} \delta_{\alpha\beta}. \quad (3.6)$$

We use this relation in the next subsection to develop the theory of characters.

3.2.4 Characters

Two representations $\mathbf{D}^{(1)}$ and $\mathbf{D}^{(2)}$ of a group G are said to be *equivalent* if they can be related by a similarity transformation of the form

$$S \mathbf{D}^{(1)} S^{-1} = \mathbf{D}^{(2)}(g), \quad (3.7)$$

where S is an appropriate matrix. The fact that equivalent representations are interchangeable suggests that each representation contains inessential information. In enumerating the possible representations of a group, we therefore only wish to consider inequivalent representations and in order to do this, require a characterisation of the representation which is invariant under similarity transformations. We find that some of the essential information of a particular representation is carried in the trace of the representation and is known as the character $\chi(g)$. If \mathbf{D} is a representation of a group, the character χ_D of \mathbf{D} is defined as

$$\chi_D(g) = \text{Trace}[\mathbf{D}(\mathbf{g})]. \quad (3.8)$$

Characters are the same for equivalent representations and similarly, elements that belong to the same conjugacy class have the same character. From the orthogonality relation stated in Eq. 3.6, we can derive an orthogonality relation for characters. By setting $i = j$ and $k = l$, we obtain

$$\sum_g \chi_{d(\alpha)}^\alpha(g)^* \chi_{d(\beta)}^\beta(g) = |G| \delta_{\alpha\beta}. \quad (3.9)$$

Let \mathbf{D} be a reducible representation of G as defined in Eq. 3.5. By taking the trace of this equation, we find

$$\chi_D(g) = m_1 \chi_{d(1)}(g) + m_2 \chi_{d(2)}(g) + \dots + m_N \chi_{d(N)}(g). \quad (3.10)$$

Multiplying Eq. 3.10 by $\chi_{d(1)}^*$ and using the orthogonality relation Eq. 3.9, we obtain the number of times (m_k) that each irreducible representation occurs within the representation $\mathbf{D}(\mathbf{g})$

$$m_1 = \frac{1}{|G|} \sum_g \chi_{d(1)}^*(g) \chi_D(g), \quad (3.11)$$

and similarly for m_2, \dots, m_N . This relation can then be used to decompose each of the representations of $O_{\sigma\mu\nu}$ and $O_{\sigma\mu\mu}$ into irreducible representations of \mathcal{H}_4 .

3.3 Decomposition of $O_{\sigma\mu\nu}$ and $O_{\sigma\mu\mu}$ into irreducible representations of \mathcal{H}_4

As stated previously, we would like to determine how each set of operators $O_{\sigma\mu\nu}$ and $O_{\sigma\mu\mu}$ with $\sigma \neq \mu \neq \nu \neq \sigma$, transforms under the hypercubic group and to decompose each of the two representations into irreducible representations of \mathcal{H}_4 .

The hypercubic group is generated by 90° rotations and reflections in each of the six lattice planes. It has 384 elements which are classified in terms of 20 conjugacy classes [50]. Each element of the group can be described as an element of the four dimensional rotation group, as an element of $SU(2) \otimes SU(2)/Z_2$ or, as a product of permutations of lattice axes with reflections along axes. For our purposes, we restrict ourselves to the final description but illustrate the connection with an example of the relation between a rotation and a permutation/reflection: $R_{12}(\frac{\pi}{2}) \equiv P_1(12)$, shown below in Fig. 3.1. The rotation is about the 3 axis (anti-clockwise in the direction of the axis), (12) denotes a permutation of the 1-2 axes and P_1 is a reflection of the 1-axis in the 2-3 plane.

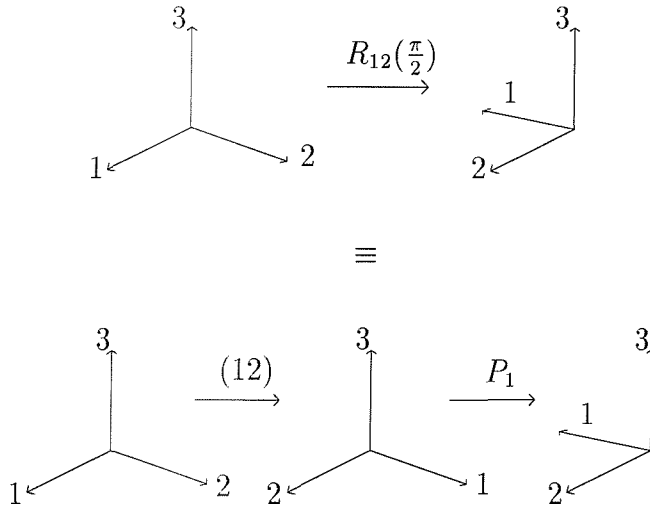


Figure 3.1: Equivalence between an element of the hypercubic group in four dimensional rotation notation and lattice permutation/reflection notation.

An example of a typical element for each conjugacy class of the hypercubic group, together with the order of each class is given in Table B.1. These elements will be used to act on the components of each basis which will then provide us with the characters of the representation (see Sec. B.2 for further explanation). The characters of the 20 irreducible representations of the hypercubic group are displayed in Tables 5.2a-c, Ref.[50].

Using this information and Eq. 3.11, we now search for the necessary Lorentz structure for both operators such that each will transform irreducibly under the hypercubic group.

3.3.1 Transformation of $O_{\sigma\mu\nu}$ under \mathcal{H}_4

We begin with the operator $O_{\sigma\mu\nu} = \bar{\psi} \gamma_\sigma \gamma_5 \overset{\leftrightarrow}{D}_\mu \overset{\leftrightarrow}{D}_\nu \psi$, with $\sigma \neq \mu \neq \nu \neq \sigma$. This is a 24-dimensional representation since there are 4 choices for σ , 3 choices for μ and 2 choices for ν . In order to obtain the characters for this representation, we must use its transformation properties under elements from each conjugacy class of the hypercubic group. The left hand column in Table B.2 displays the components of the basis vector for this representation which are constructed from the direct product of p_μ , q_ν and r_σ , where each of these objects transforms like a vector under \mathcal{H}_4 . The elements of the group then act on each component in this column vector according to the rules given in Sec. B.2. Subsequent columns display the transformation properties under an element from each conjugacy class. The sum of each column is given at the base of Table B.2, thus we obtain the character of the representation for each element.

Combining the results from Table B.2 with characters of the irreducible representations of \mathcal{H}_4 ² and using the character orthogonality relation (Eq. 3.11), we

²The characters of the irreducible representations of \mathcal{H}_4 are given in Tables 5.2a-c, Ref.[50].

establish how many times (m_k) each irreducible representation occurs within the 24-dimensional reducible representation. We find that $O_{\sigma\mu\nu}$ transforms like a $(\frac{1}{2}, \frac{1}{2})^{(+)} \oplus (\overline{\frac{1}{2}}, \overline{\frac{1}{2}})^{(+)} \oplus \mathbf{2.8}^{(+)}$ reducible representation. However, if we consider the combination $O_{\sigma\{\mu\nu\}}$, with $\sigma \neq \mu \neq \nu \neq \sigma$ and symmetrising over μ and ν , we obtain a 12 dimensional representation (Table B.4), which transforms like a $(\overline{\frac{1}{2}}, \overline{\frac{1}{2}})^{(+)} \oplus \mathbf{8}^{(+)}$ reducible representation.

3.3.2 Transformation of $O_{\sigma\mu\mu}$ under \mathcal{H}_4

The second operator $O_{\sigma\mu\mu} = \bar{\psi} \gamma_\sigma \gamma_5 \overset{\leftrightarrow}{D}_\mu \overset{\leftrightarrow}{D}_\mu \psi$, with $\sigma \neq \mu$ is a 12 dimensional representation since there are four choices for σ and three choices for μ . The components of the basis vector are displayed in the left hand column of Table B.3 and are constructed (as in the previous case with the exception that $\mu = \nu$) by taking the direct product of $q_\sigma \otimes p_\mu \otimes p_\mu$, where q_σ and p_μ are four vectors. As before, the characters of the representation are established from the transformation properties of the operator under different elements in the hypercubic group. Using the character orthogonality relation (Eq. 3.11) to combine the results from Table B.3 with the irreducible representations of \mathcal{H}_4 , we find that it transforms like a $(\frac{1}{2}, \frac{1}{2})^{(-)} \oplus \mathbf{8}^{(-)}$ reducible representation.

In order to isolate a particular irreducible representation for each operator, we try to construct a basis that will transform like the $\mathbf{8}^{(-)}$ dimensional irreducible representation. From Table B.5 we find that the linear combination $p_\sigma \left[p_\tau^2 - \frac{p_\nu^2 + p_\mu^2}{2} \right]$ transforms as required and so we are able to isolate the irreducible representations of each operator that will not mix with lower dimensional operators.

3.4 Summary

The operator $O_{\sigma\{\mu\nu\}} = \bar{\psi} \gamma_\sigma \gamma_5 \overset{\leftrightarrow}{D}_\mu \overset{\leftrightarrow}{D}_\nu \psi$ with $\sigma \neq \mu \neq \nu \neq \sigma$ and symmetrising over μ and ν transforms like a $(\frac{1}{2}, \frac{1}{2})^{(+)} \oplus \mathbf{8}^{(+)}$ reducible representation of the hypercubic group, which does not mix with lower dimensional operators. In order to obtain an operator proportional to $p_\sigma p_\mu p_\nu$, as in the continuum limit, the $\mathbf{8}^{(+)}$ term must be subtracted. However, this term vanishes when we take the matrix element of this operator between the pion and the vacuum since there is only one four-momentum from which to build the $\mathbf{8}^{(+)}$ term. Thus we obtain the term that is directly proportional to the second moment of the pion's distribution amplitude,

$$\langle 0 | O_{\sigma\{\mu\nu\}} | \pi(p) \rangle = A p_\sigma p_\mu p_\nu, \quad (3.12)$$

where p is the four momentum of the pion and the coefficient A is proportional to $\langle \xi^2 \rangle$. In order to obtain a non-vanishing signal, this choice of Lorentz indices requires two non-zero components of the spatial momentum.

The operator $O_{\sigma\mu\mu} = \bar{\psi} \gamma_\sigma \gamma_5 \overset{\leftrightarrow}{D}_\mu \overset{\leftrightarrow}{D}_\mu \psi$ with $\sigma \neq \mu$ transforms like the $(\frac{1}{2}, \frac{1}{2})^{(-)} \oplus \mathbf{8}^{(-)}$ reducible representation of the hypercubic group. In order to prevent mixing with lower dimensional operators, a linear combination of these operators is taken and we find that the subtracted operator

$$O'_{411} = O_{411} - \frac{O_{422} + O_{433}}{2} \quad (3.13)$$

transforms like the $8^{(-)}$ irreducible representation. Taking the matrix element of the operator defined in Eq. 3.13 between the pion and the vacuum,

$$\langle 0 | O'_{411} | \pi(p) \rangle = C p_4 \left[p_1^2 - \frac{p_2^2 + p_3^2}{2} \right], \quad (3.14)$$

we are able to isolate the term containing $\langle \xi^2 \rangle$. This combination of indices allows for just one non-zero component of the spatial momentum.

Chapter 4

Operator Matching

The lattice formulation is a bare theory which is regularised by an ultra-violet cut-off a^{-1} (in momentum space). The results obtained for bare lattice operators must therefore be translated to those of renormalised ones, and this is done by “matching” them onto a continuum renormalisation scheme, e.g. the $\overline{\text{MS}}$ scheme. The motivation behind this lies in the fact that the renormalisation scale and scheme dependence must be removed in order to obtain physical results. Since the Wilson coefficients that remove this dependence are usually computed in the $\overline{\text{MS}}$ scheme, the results obtained from lattice calculations must be related to this scheme. Furthermore, the results for the second moment using QCD sum rules are defined in this scheme and therefore, matching is necessary to obtain a result that can be compared with sum rule predictions.

In this chapter, we examine how these matching coefficients are computed at one-loop to obtain a result in the $\overline{\text{MS}}$ scheme. We discuss the details and present the results of the perturbation theory used to obtain the matching coefficients. This requires the calculation of one-loop Feynman diagrams both on the lattice and in the continuum.

4.1 Matching to the $\overline{\text{MS}}$ scheme

As discussed in Ch. 2, lattice operators are defined with a cut-off a , denoted in this chapter as $Q(a)$. There are several ways in which to compute the matching coefficients for $Q(a)$. One technique is that of non-perturbative renormalisation [51]. In comparison with perturbative matching, the systematic effects are different but it is easier to control them. Since the renormalisation constants relevant to this quantity have not been computed non-perturbatively, we resort to perturbation theory at the one-loop level.

The form of the matrix element of the relevant operator Q_i at one-loop, both in the continuum and on the lattice, is given by

$$\langle Q_i \rangle_{\overline{\text{MS}}, \text{latt}} = Z_{\overline{\text{MS}}, \text{latt}} \langle Q_i \rangle^{(0)}, \quad (4.1)$$

where $\langle Q_i \rangle^{(0)}$ is the tree level matrix element of Q_i sandwiched between the relevant external states, and $Z_{\overline{\text{MS}}, \text{latt}}$ are the one-loop renormalisation constants. Since matrix elements must be the same in all regularisation schemes at tree-level, we define the matching condition:

$$Z_{\overline{\text{MS}}}^{-1} \langle Q_i \rangle_{\overline{\text{MS}}} = Z_{\text{latt}}^{-1} \langle Q_i \rangle_{\text{latt}}. \quad (4.2)$$

For the composite operators relevant to this work, the renormalisation constants are of the form

$$Z_{\overline{\text{MS}}} = 1 + \frac{\alpha_s}{4\pi} [\gamma^{(0)} \log \left(\frac{\mu^2}{\lambda^2} \right) + d_{\text{cont}}], \quad (4.3)$$

$$Z_{\text{latt}} = 1 + \frac{\alpha_s}{4\pi} [\gamma^{(0)} \log \left(\frac{1}{a^2 \lambda^2} \right) + d_{\text{latt}}], \quad (4.4)$$

where $\gamma^{(0)}$ is the one-loop anomalous dimension associated with the operator Q_i

and is universal i.e. it has the same value in all regularisation schemes. The logarithmic terms in Eqs. 4.3 and 4.4 arise from the regularisation of UV divergences, and the constants d_{cont} and d_{latt} are finite contributions which are scheme-dependent. In the presence of an IR divergence, the same regulator must be used in the calculation of $Z_{\overline{\text{MS}}}$ and Z_{latt} for the purpose of matching. In this work, a gluon mass λ is included in the gluon propagator (see App. C.1 for the Feynman rules) to regulate the IR divergence. Having defined the one-loop correction in Eq. 4.1, the matching coefficient Z_M is then defined as

$$\begin{aligned} Z_M &\equiv \left(\frac{Z_{\overline{\text{MS}}}}{Z_{\text{latt}}} \right) \\ &= 1 + \frac{\alpha}{4\pi} [\gamma^{(0)} \log(a^2 \mu^2) + (d_{\text{cont}} - d_{\text{latt}})]. \end{aligned} \quad (4.5)$$

We note that the dependence on the IR regulator has cancelled in Eq. 4.5.

4.2 Perturbation theory

4.2.1 Continuum perturbation theory

In this section, we present the results for the one-loop perturbation theory in the continuum. The Feynman rules are given in App. C.1.1 and the one-loop diagrams, computed in the Feynman gauge, are illustrated in App. C.2. The one-loop correction from each diagram is given in Table 4.1. We note that the one-loop correction from the self energy is that for the wavefunction renormalisation. The three results are summed together to obtain a value for Z_{latt} .

In the continuum Feynman rules, we note the absence of a rule containing the operator $O_{\sigma\mu\mu}$ that is proportional to g^2 . In fact, all the diagrams in the contin-

diagram	one-loop correction
self energy	$\frac{\alpha_s}{4\pi} C_F \left[-\log C - \frac{1}{2} \right]$
$O_{\sigma\mu\nu}$	
$2 \times \text{sail}(A + B)$	$\frac{\alpha_s}{4\pi} C_F \left[-\frac{10}{3} \log C - \frac{13}{9} \right]$
vertex correction	$\frac{\alpha_s}{4\pi} C_F \left[\frac{1}{6} \log C - \frac{29}{144} \right]$

Table 4.1: One-loop results from the continuum, where $C = \frac{\mu^2}{\lambda^2}$ and $C_F = \frac{4}{3}$.

uum are the same for each operator. The two-gluon diagram does not exist for $O_{\sigma\{\mu\nu\}}$ since $\mu \neq \nu$. The reason this term is also absent for $O_{\sigma\mu\mu}$ is that there are no derivatives present to build a term proportional to p_μ^2 . Therefore, the diagram containing this term is a trace term in the continuum calculation which is subtracted from the complete set of diagrams in order to isolate the second moment.

4.2.2 Lattice perturbation theory

The one-loop contribution from each diagram computed using lattice perturbation theory is presented in Table 4.2, where the numerical error in the finite contribution is less than 0.1%. The wavefunction renormalisation is defined by the correction from the self energy diagrams. The Feynman rules are given in App. C.1 and the diagrams are illustrated in App. C.2. In addition, the computation of the sail diagrams on the lattice is outlined in App. C.3.

In the lattice simulation, isolating the term that contains the second moment involves taking the ratio of the correlator of the operator with the correlator of the axial current. Since chiral symmetry is broken on the lattice, the axial current will also get renormalised and we state here the one-loop contribution to the axial current [52],

diagram	one-loop correction
self energy	$\frac{\alpha}{4\pi} C_F [-\log L + 1.12]$
$2 \times$ self energy (clover)	$\frac{\alpha}{4\pi} c_{SW} C_F (-2.249)$
self energy (clover-clover)	$\frac{\alpha}{4\pi} c_{SW}^2 C_F (0.458)$
tadpole correction	$\frac{\alpha}{4\pi} C_F (-12.24)$
$O_{\sigma\mu\nu}$	
$2 \times$ sail($A + B$)	$\frac{\alpha}{4\pi} C_F [-\frac{10}{3} \log L - 2.171]$
$2 \times$ sail($A + B$) (clover)	$\frac{\alpha}{4\pi} C_F c_{SW} (2.689)$
vertex correction	$\frac{\alpha}{4\pi} C_F [\frac{1}{6} \log L - 0.018]$
$2 \times$ vertex (clover)	$\frac{\alpha}{4\pi} C_F c_{SW} (-3.26)$
vertex (clover-clover)	$\frac{\alpha}{4\pi} C_F c_{SW}^2 (-0.793)$
$O_{\sigma\mu\mu}$	
$2 \times$ sail($A + B$)	$\frac{\alpha}{4\pi} C_F [-\frac{10}{3} \log L + 1.611]$
$2 \times$ sail($A + B$) (clover)	$\frac{\alpha}{4\pi} C_F c_{SW} (-0.672)$
vertex correction	$\frac{\alpha}{4\pi} C_F [\frac{1}{6} \log L - 1.979]$
$2 \times$ vertex (clover)	$\frac{\alpha}{4\pi} C_F c_{SW} (-0.476)$
vertex (clover-clover)	$\frac{\alpha}{4\pi} C_F c_{SW}^2 (3.92)$
tadpole ($O_{\sigma\mu\mu}$)	$\frac{\alpha}{4\pi} C_F (48.932)$

Table 4.2: One-loop results from the lattice, where $L = \frac{1}{(a^2 \lambda^2)}$ and $C_F = \frac{4}{3}$.

$$Z_A = 1 + \frac{\alpha_s}{4\pi} C_F \left[-15.796 - 0.248 c_{SW} + 2.251 c_{SW}^2 \right]. \quad (4.6)$$

The renormalisation constant Z_A is computed in this work with $c_{SW} = 1$.

4.3 The matching procedure and associated uncertainties

In the one-loop matching procedure, the choice of coupling constant used and the scale at which the matching is performed must be carefully considered. We now discuss these options before computing the coefficients in Eq. 4.5.

- In performing operator matching using a perturbative expansion to one-loop, one is free to choose the expansion parameter α_s , defined as

$$\alpha_s = \frac{g^2}{4\pi}. \quad (4.7)$$

Choosing the bare lattice coupling as the expansion parameter often gives poor convergence of the series. A better choice is that of the “boosted” coupling constant [53]:

$$\alpha_{\text{boosted}} = \frac{6}{\beta u_0^4 4\pi}, \quad (4.8)$$

where $u_0 = \left\langle \frac{1}{3} \text{Tr} U_{\text{plaq}} \right\rangle^{1/4}$ is the gauge invariant mean value of U_μ , and β is the same parameter that appears in the Wilson plaquette action which is related to the bare coupling by

$$g_0^2 = \frac{6}{\beta}. \quad (4.9)$$

In addition to the boosted coupling, another favourable choice of α_s is that of the $\overline{\text{MS}}$ scheme as described in Ref. [53]. Following this proposal, we use u_0 which is measured numerically on the lattice, and the relation

$$-\ln(u_0) = \frac{\pi}{3} \alpha_v(3.41/a)(1 - 1.185\alpha_v), \quad (4.10)$$

where the coupling $\alpha_v(3.41/a)$ [54] is defined from the heavy quark potential [55]. Solving Eq. 4.10 for $\alpha_v(3.41/a)$, and using the relation [56]

$$\alpha_{\overline{\text{MS}}} \left(\frac{3.41}{a} \right) = \alpha_v(e^{5/6} 3.41/a)(1 + \frac{2\alpha_v}{\pi} + C_2^{(n_f)} \alpha_v^2), \quad (4.11)$$

we then obtain $\alpha_{\overline{\text{MS}}}$ by running α_v at the two-loop level, with number of flavours $n_f = 0$ (quenched approximation). Using the same two-loop

running, $\alpha_{\overline{\text{MS}}}(q)$ is then computed at different scales. In this work, the simulation uses $\beta = 6.2$ and the corresponding $u_0 = 0.8771$. A central value for Z_M is obtained by using $\alpha_{\overline{\text{MS}}}(q = 2/a)$. By varying q between $1/a$ and π/a , the systematic errors are estimated. The numerical values of $\alpha_{\overline{\text{MS}}}(q)$ at $q = 1/a, 2/a$ and π/a are given in Table 4.3.

β	$\alpha_{\overline{\text{MS}}}(1/a)$	$\alpha_{\overline{\text{MS}}}(2/a)$	$\alpha_{\overline{\text{MS}}}(\pi/a)$
6.2	0.172993	0.140189	0.124985

Table 4.3: The variation of $\alpha_{\overline{\text{MS}}}(q)$ with scale that will be used in the one-loop matching procedure

- The scheme-dependent constants d_{cont} and d_{latt} are next-to-leading logarithms and can be absorbed by tuning the scale μ . However, since this can result in a loss of control over the higher order logarithmic contributions, μ is usually chosen to be of $O(1/a)$, thus maintaining a small contribution from these terms.
- The choice of c_{SW} affects the value of d_{latt} in Eq. 4.4. In this work, we use $c_{SW} = 1$ in the one-loop matching as the clover term is always accompanied by powers of α_s in the perturbative calculation.

4.4 Results

We now present the results for Z_M/Z_A with different values of α_s . The numerical results for each operator are displayed in Table 4.4 where Z_M/Z_A is given for various α_s with $a\mu = 1$ and $c_{SW} = 1$.

Z_M/Z_A	α_s			
	0.1255 (boosted)	0.12499 ($q = \pi/a$)	0.14019 ($q = 2/a$)	0.17299 ($q = 1/a$)
$Z_1 (O_{\sigma\mu\nu})$	1.451	1.449	1.518	1.680
$Z_2 (O_{\sigma\mu\mu})$	0.556	0.558	0.490	0.331

Table 4.4: Matching coefficients for different α_s with $C_{SW} = 1.0$ and $a\mu = 1.0$.

Chapter 5

Numerical simulation, analysis and results

In Ch. 3, we established the form of the operators which, when sandwiched between the pion and the vacuum, yield the second moment of the pion's distribution amplitude $\langle \xi^2 \rangle$. Following this, the one-loop matching coefficients were computed in order to relate the lattice results to the $\overline{\text{MS}}$ scheme (Ch. 4). In this chapter, we present the details of the numerical simulation of the correlators that contain these matrix elements. The numerical results are then matched to the $\overline{\text{MS}}$ scheme and the systematic errors associated with the final results are discussed.

5.1 Lattice computation

In this section, we state the details of the lattice on which the simulation was performed. The correlation functions that were computed are listed and we examine how they are combined such that $\langle \xi^2 \rangle$ is isolated.

5.1.1 Simulation details

The details of the simulation are summarised in the following:

- $\beta = \frac{6}{g_0^2} = 6.2$ (where g_0 is the bare coupling), with corresponding inverse lattice spacing $a^{-1} = 2.67 \pm 0.06 \text{ GeV}$ (from the spectrum results for m_{K^*} [57] using r_0 as determined in Ref. [58]), on a $24^3 \times 48$ lattice;
- SW fermion action, with $c_{SW} = 1.61$, tuned such that the action is non-perturbatively improved with all $O(a)$ errors removed;
- the three values of κ used in the simulation are shown with the corresponding physical light pseudoscalar masses (composed of degenerate quarks) in Table 5.1, with $\kappa_c = 0.135818_{-14}^{+17}$ [57];

κ	$\kappa = 0.13460$	$\kappa = 0.13510$	$\kappa = 0.13530$
$M_{\text{ps}} \text{ (MeV)}$	748_{-2}^{+4}	574_{-4}^{+5}	490_{-5}^{+6}

Table 5.1: Values of κ shown with the corresponding values of pseudoscalar meson mass [58] (converted into natural units using $a^{-1} = 2.67 \text{ GeV}$), obtained by fitting to Eq. 5.10.

- the 154 quenched configurations used in the simulation were generated using an over-relaxed [59, 60] Cabibbo-Marinari algorithm [61], and the quark propagators were generated using the bi-Conjugate Gradient Stab algorithm [62];
- non-improved local operators;
- the statistical error in this work is estimated by creating 100 bootstrap samples.

5.1.2 Correlation functions

The matrix elements that yield $\langle \xi^2 \rangle$ are

$$\langle 0 | O_{\sigma\{\mu\nu\}} | \pi(p) \rangle = f_\pi \langle \xi^2 \rangle p_\sigma p_\mu p_\nu, \quad (5.1)$$

$$\langle 0 | O'_{\sigma\mu\mu} | \pi(p) \rangle = f_\pi \langle \xi^2 \rangle p_\sigma p_\mu p_\mu, \quad (5.2)$$

where f_π is the pion decay constant.

Generically, for an operator Q , the two-point correlator can be written as

$$C_2^Q(\mathbf{p}, t) = \sum_{\mathbf{x}} e^{i\mathbf{p}\cdot\mathbf{x}} \langle Q(\mathbf{x}, t) \Phi^\dagger(0) \rangle, \quad (5.3)$$

where \mathbf{p} is the spatial momentum and $\Phi = \bar{\psi} \gamma_5 \psi$ (typically of the form $\bar{u} \gamma_5 d$) is the interpolating operator which overlaps with the single pion state. Inserting a complete set of states and considering large Euclidean time separation that ensures dominance of the ground state, Eq. 5.3 can be re-expressed as

$$C_2^Q(\mathbf{p}, t) \xrightarrow{t \rightarrow \infty} \frac{Z_\pi}{2E_\pi} \langle 0 | Q(0) | \pi(\mathbf{p}) \rangle e^{-E_\pi t}, \quad (5.4)$$

where E_π is the energy of the pion, and Z_π is the wavefunction renormalisation given by

$$Z_\pi = \langle 0 | \bar{\psi} \gamma_5 \psi | \pi \rangle, \quad (5.5)$$

which is independent of \mathbf{p} . We now list the two-point functions that are combined in order to compute $\langle \xi^2 \rangle$. This includes the pion propagator,

$$C_2^5(\mathbf{p}, t) = \sum_{\mathbf{x}} e^{i\mathbf{p}\cdot\mathbf{x}} \langle 0 | \Phi(\mathbf{x}, t) \Phi^\dagger(0) | 0 \rangle, \quad (5.6)$$

In isolating $\langle \xi^2 \rangle$, it is necessary to compute the correlator composed of the fourth component of the axial current A_μ and the interpolating operator Φ^1

$$C_2^A(\mathbf{p}, t) = \sum_{\mathbf{x}} e^{i\mathbf{p}\cdot\mathbf{x}} \langle 0 | A_4(\mathbf{x}, t) \Phi^\dagger(0) | 0 \rangle. \quad (5.7)$$

The correlators involving the two operators appearing in Eqs. 5.1 and 5.2 are defined as

$$C_2^O(\mathbf{p}, t) = \sum_{\mathbf{x}} e^{i\mathbf{p}\cdot\mathbf{x}} \langle 0 | O_{\sigma\{\mu\nu\}}(\mathbf{x}, t) \Phi^\dagger(0) | 0 \rangle, \quad (5.8)$$

$$C_2^{O'}(\mathbf{p}, t) = \sum_{\mathbf{x}} e^{i\mathbf{p}\cdot\mathbf{x}} \langle 0 | O'_{\sigma\mu\mu}(\mathbf{x}, t) \Phi^\dagger(0) | 0 \rangle. \quad (5.9)$$

Inserting a complete set of states and looking at large Euclidean time separations, the above correlators can be written as

$$C_2^5(\mathbf{p}, t) = \frac{Z_\pi^2}{2E_\pi} [e^{-E_\pi t} + e^{-E_\pi(T-t)}], \quad (5.10)$$

$$C_2^A(\mathbf{p}, t) = \frac{Z_\pi}{2} f_\pi e^{-E_\pi t}, \quad (5.11)$$

$$C_2^O(\mathbf{p}, t) = \frac{Z_\pi}{2E_\pi} e^{-E_\pi t} f_\pi \langle \xi^2 \rangle p_\sigma p_\mu p_\nu, \quad (5.12)$$

$$C_2^{O'}(\mathbf{p}, t) = \frac{Z_\pi}{2E_\pi} f_\pi \langle \xi^2 \rangle p_\sigma p_\mu p_\nu e^{-E_\pi t}, \quad (5.13)$$

where we remind the reader that

$$O'_{411} = O_{411} - \frac{O_{422} + O_{433}}{2}, \quad (5.14)$$

as defined in Ch. 3. We also note that σ is chosen to be the time direction. The second moment is isolated by taking the ratio of the correlator containing the operator $O_{\sigma\{\mu\nu\}}$ or $O'_{\sigma\mu\mu}$ with $C_2^A(\mathbf{p}, t)$ (computed at the same spatial momentum).

¹This is done in order to compute the pion decay constant f_π which is then divided out.

For $O_{\sigma\{\mu\nu\}} = O_{4\{12\}}$,

$$\begin{aligned} R_1 &= \left. \frac{C_2^O(t)}{C_2^A(t)} \right|_{\mathbf{p}=(1,1,0)} \\ &= p_1 p_2 \langle \xi^2 \rangle \end{aligned} \quad (5.15)$$

In the case of $O'_{\sigma\mu\mu} = O'_{411}$, we define

$$\begin{aligned} R_2 &= \left. \frac{C_2^{O'}(t)}{C_2^A(t)} \right|_{\mathbf{p}=(1,0,0)} \\ &= p_1^2 \langle \xi^2 \rangle. \end{aligned} \quad (5.16)$$

We note that in the above equations, R_1 (R_2) correspond to R_2 (R_1) in the notation of Ref. [7].

By exploiting the cubic symmetry of the lattice, R_1 and R_2 are computed in different directions of the momentum. The final results quoted for R_1 and R_2 are averages of those related by cubic symmetry.

5.2 Analysis and lattice results

Having defined the correlators, we now present the details of the numerical analysis and results.

5.2.1 Correlators and Plateaux

In this section, we first present the effective mass plots, obtained using

$$E_{\text{eff}} = -\log \frac{C_2^5(\mathbf{p}, t+1)}{C_2^5(\mathbf{p}, t)}. \quad (5.17)$$

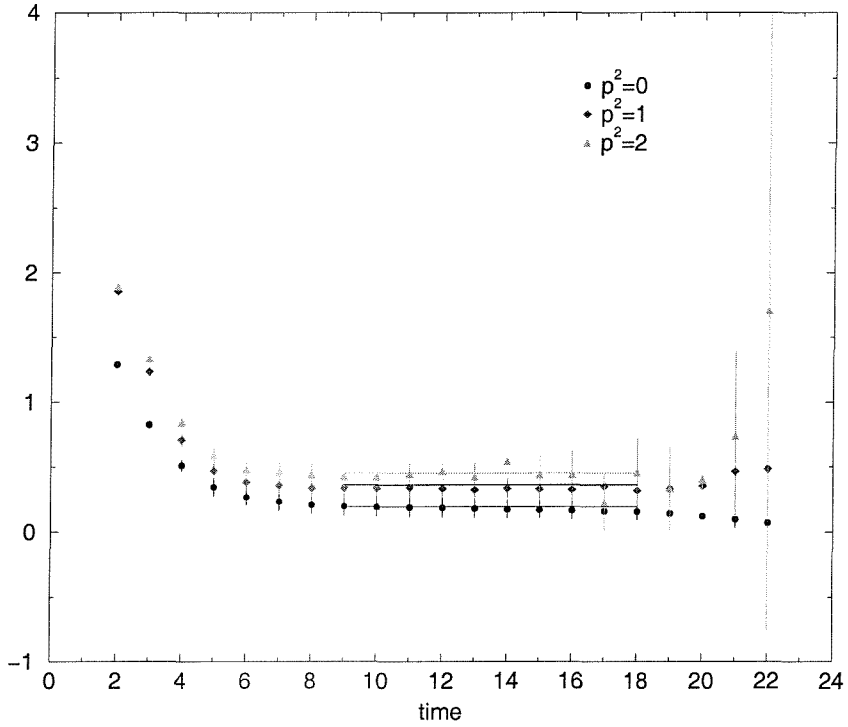


Figure 5.1: Effective mass plot for $\kappa = 0.13530$. Each fit is an estimate for the energy of the pion (as in Eq. 5.17), and for $\mathbf{p}^2 = 0$, we obtain a value for the mass of the pion.

These are used to estimate the range over which to fit R_1 and R_2 to a constant. As a typical example, the effective mass plot for $\kappa = 0.13530$ is presented in Fig. 5.1. From this plot, the range over which it is assumed that the single pion state has been isolated is estimated to be $9 < t < 18$ (for all spatial momenta).

The correlator $C_2^A(\mathbf{p}, t)$ (the fourth component of the axial current), is presented in Fig. 5.2, using a logarithmic scale with $\kappa = 0.13460$, and momentum $\mathbf{p}^2 = 1$ and $\mathbf{p}^2 = 2$.

Before presenting the final plateaux for R_1 and R_2 , we display the individual results for each direction. The purpose of this is to ensure that the results are compatible and therefore independent of direction, i.e., that cubic symmetry is

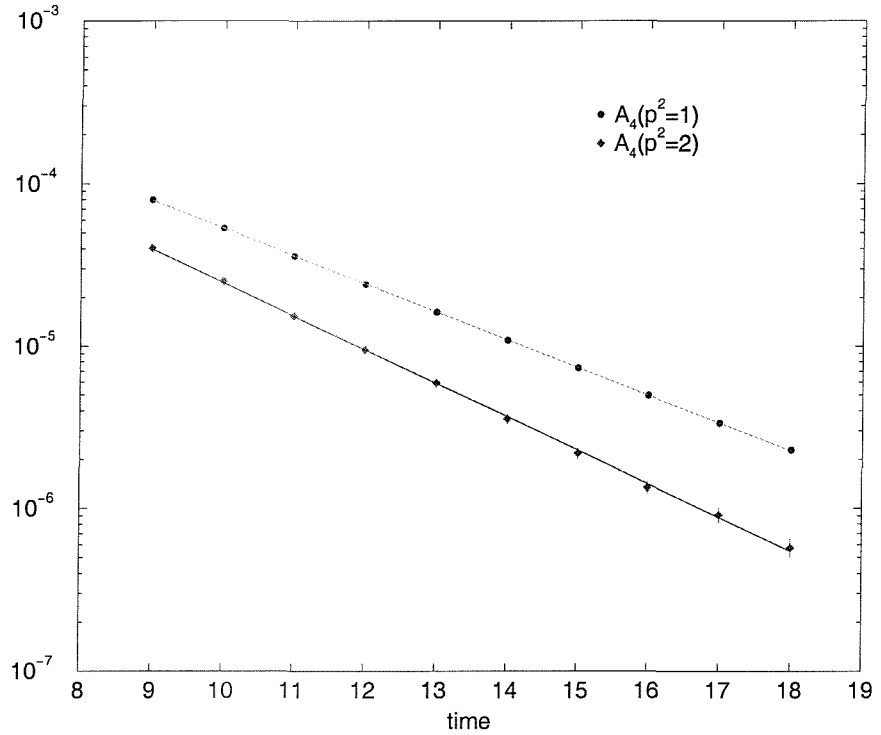


Figure 5.2: The fourth component of the axial current plotted on a logarithmic scale at $p^2 = 1$ and $p^2 = 2$, for $\kappa = 0.13460$. The straight-line behaviour of each set indicates that the data points fit well to an exponential.

maintained. Fig. 5.3 displays the results for R_1 computed in different directions on the lattice. The results for R_2 are given in Fig. 5.4.

Having selected a suitable range, we now present the average of the individual results for R_1 and R_2 in Fig. 5.5, where both plots are computed with $\kappa = 0.13460$. Fitting R_1 and R_2 to a constant, we obtain the results presented in Table 5.2.

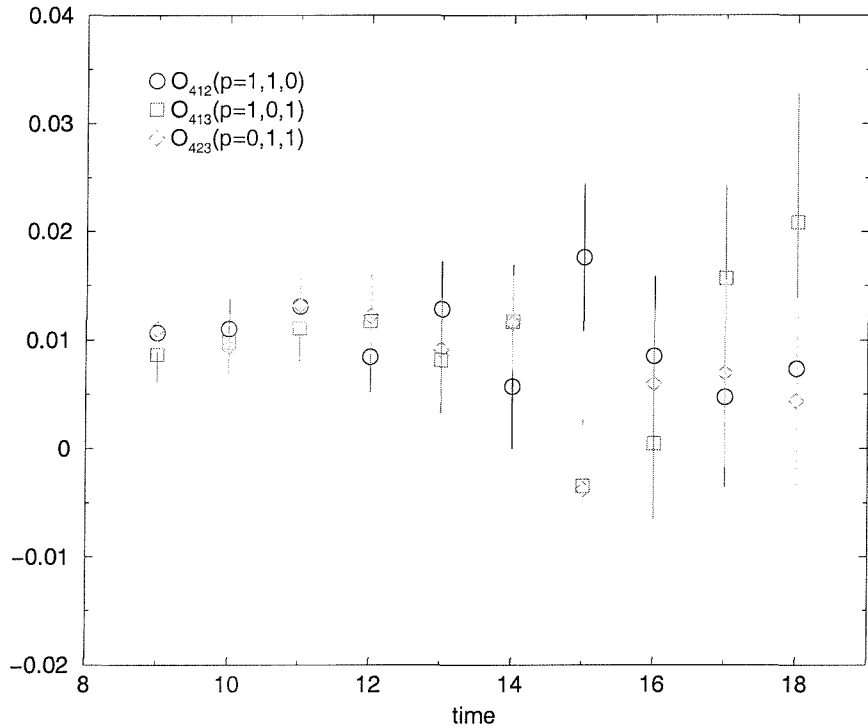


Figure 5.3: R_1 ($O_{\sigma[\mu\nu]}$) computed in different directions ($p^2 = 2$).

5.2.2 Numerical results

In Sec. 5.2.1, we presented the results for R_1 , R_2 at different κ . In order to obtain values in the limit of zero quark mass, the results given in Table 5.2 must be extrapolated to κ_{crit} . Each extrapolation for R_1 and R_2 is shown in Fig. 5.6.

Extrapolating $\langle \xi^2 \rangle$ to the zero quark mass limit, we find the bare lattice results:

$$\langle \xi^2 \rangle_{L_1} = 0.1845 \pm 0.0322 \quad (\text{from } R_1) \quad (5.18)$$

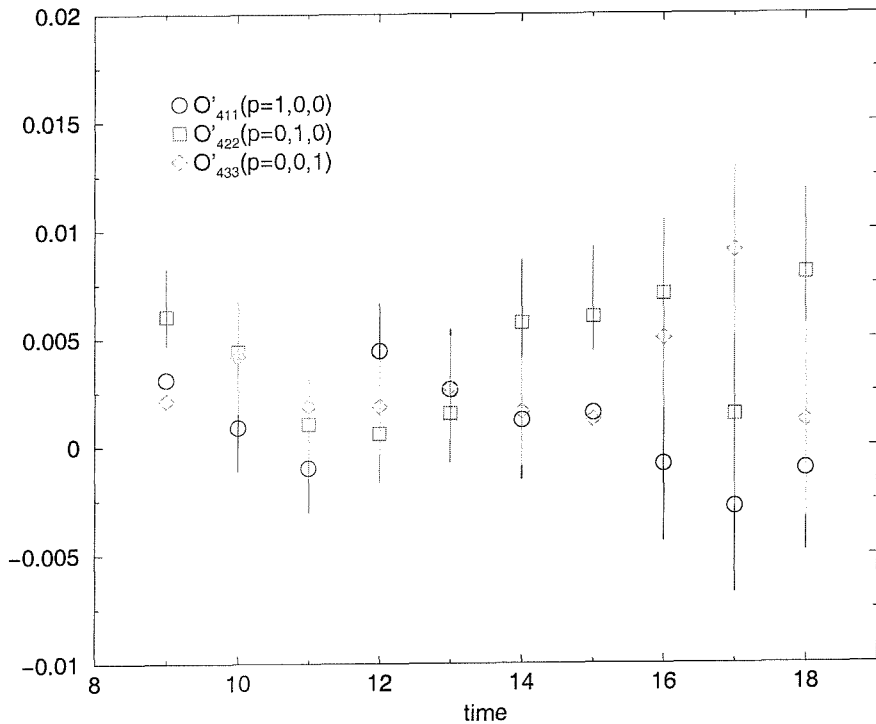


Figure 5.4: R_2 ($O'_{\sigma\mu\mu}$) computed in different directions ($p^2 = 1$).

and

$$\langle \xi^2 \rangle_{L_2} = 0.0436 \pm 0.0170 \quad (\text{from } R_2) \quad (5.19)$$

5.3 Final results and systematic errors

In this section, we present the result for $\langle \xi^2 \rangle$ in the $\overline{\text{MS}}$ scheme and discuss the systematic errors.

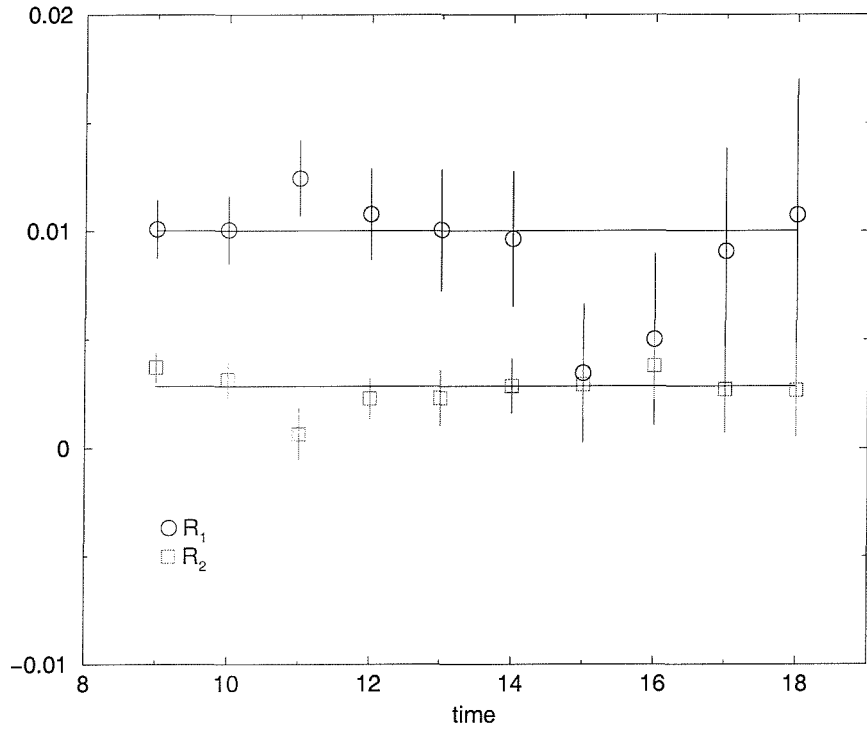


Figure 5.5: R_1 ($O_{\sigma[\mu\nu]}$) and R_2 ($O'_{\sigma\mu\mu}$) with $\kappa = 0.13460$.

5.3.1 Results in the $\overline{\text{MS}}$ scheme

Having obtained $\langle \xi^2 \rangle$ in the lattice regularisation scheme, we must now match the results onto the $\overline{\text{MS}}$ scheme,

$$\langle \xi^2 \rangle_{\overline{\text{MS}}} = (Z_O/Z_A)\langle \xi^2 \rangle_L, \quad (5.20)$$

where Z_O is the matching coefficient which relates the lattice operator O_L , to its $\overline{\text{MS}}$ counterpart, and Z_A is the renormalisation constant for the axial current.

R_n	$\kappa = 0.13460$	$\kappa = 0.13510$	$\kappa = 0.13530$
R_1	0.010018 ± 0.000714	0.011018 ± 0.001192	0.011658 ± 0.001720
R_2	0.002854 ± 0.000359	0.003077 ± 0.000634	0.002703 ± 0.000906

Table 5.2: R_1 and R_2 for different κ

Combining the results in Sec. 5.2.2 with matching coefficients (as presented in Ch. 4), we obtain the following results:

$$\langle \xi^2 \rangle_{\overline{\text{MS}}_1} = 0.280(49)^{+30}_{-13} \quad (5.21)$$

and

$$\langle \xi^2 \rangle_{\overline{\text{MS}}_2} = 0.021(8)^{+3}_{-7} \quad (5.22)$$

where the first error quoted is statistical and the second is the systematic error. In obtaining Eqs. 5.21 and 5.22, we use the one-loop matching coefficients calculated at $\alpha_s(q = 2/a)$, $c_{SW} = 1.0$ and match at $\mu = 1/a$ which will be discussed in the next section.

5.3.2 Systematic errors

The main systematic error in this work is due to the matching coefficients computed in Chapter 4. Choosing $c_{SW} = 1.0$ (since $c_{SW} = 1.61$ is of the order α_s^2), we must then decide the value of α_s at which to perform the perturbative expansion, and the scale μ at which to match the lattice and continuum one-loop results.

Since we perform the matching at the one-loop level, there is no preferred choice of α_s . We therefore choose $\alpha_s(q)$ obtained in the $\overline{\text{MS}}$ scheme [53], as described in Sec. 4.3. We then use this coupling constant at the scale $q = 2/a$ (the central

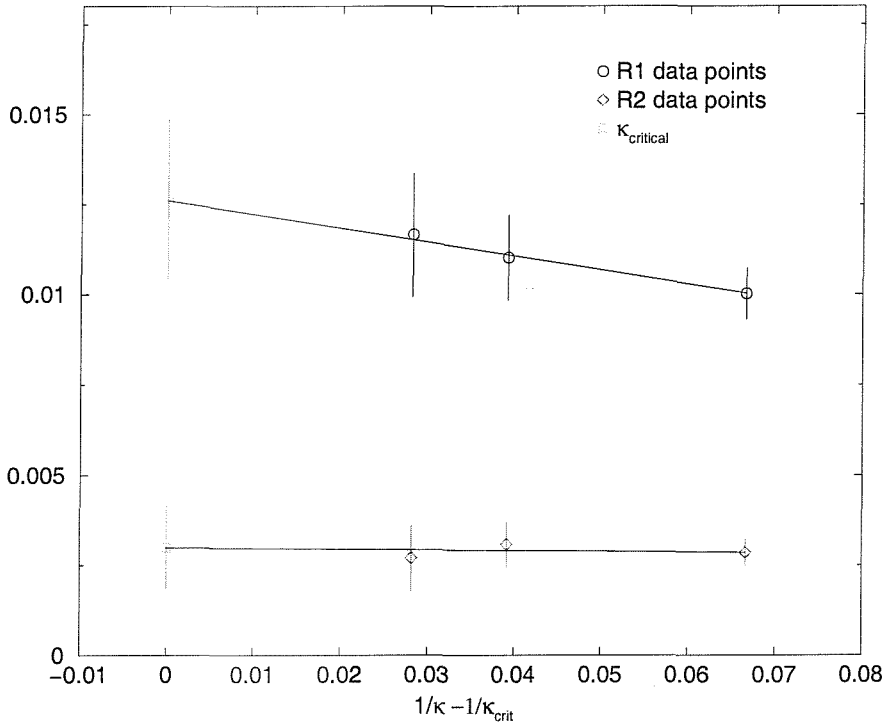


Figure 5.6: The extrapolation of R_1 and R_2 to the zero quark mass limit.

value) and vary q between $1/a$ and π/a to estimate the systematic error.

By performing the matching at $\mu = 1/a$, all the log terms vanish in the expansion. In this procedure, the leading error is of the form $(\alpha_s/4\pi)^2 k$, where k is a constant, independent of μa . Obtaining k on the lattice is a formidable task. In principle, one could calculate the two-loop anomalous dimension $\gamma_{\text{latt}}^{(1)}$ and use it to run at next-to-leading order on the lattice to another scale. Matching is then performed at one-loop and the result run back to $\mu = 1/a$ in the $\overline{\text{MS}}$ scheme at the same precision (having computed $\gamma_{\overline{\text{MS}}}^{(1)}$). The difference between this result and the one obtained by matching directly at $\mu = 1/a$ will then indicate the size of $(\alpha_s/4\pi)^2 k$.

However, in view of the fact that the one-loop correction to each operator is large (especially in the case of R_2), it is difficult to be sure of the accuracy of this approach. It would therefore be preferable to match non-perturbatively, thus removing the uncertainty that accompanies the perturbative series.

The extrapolation to $m_q = 0$ is mild, particularly in the case of R_2 , and so the error associated with it is expected to be small. Since the simulations were performed using only one value for the lattice spacing, it is not possible to extrapolate to the continuum limit. Although an improved action has been used and we are working with a light-quark system at quite a fine lattice spacing ($a^{-1} = 2.67 \pm 0.06 \text{ GeV}$), we note that it would be preferable to include improved operators in order to further reduce discretisation errors.

Finally, the results are obtained within the quenched approximation. In order to make a reliable estimate of the error due to quenching, we would have to perform a simulation using dynamical fermions which is beyond the scope of this work.

Chapter 6

Conclusions

In this work, the second moment of the pion's distribution amplitude $\langle \xi^2 \rangle$ has been computed from lattice QCD using two operators, each belonging to a different irreducible representation of the hypercubic group. The results obtained at 2.67 GeV in the $\overline{\text{MS}}$ scheme are (from Eqs. 5.21 and 5.22)

$$\langle \xi^2 \rangle_1 = 0.280(49)^{+30}_{-13}$$

and

$$\langle \xi^2 \rangle_2 = 0.021(8)^{+3}_{-7}.$$

These results are incompatible and correspond to significantly different distribution amplitudes. The value for $\langle \xi^2 \rangle_1$, obtained from R_1 (defined in Eq. 5.15), indicates that a large fraction of the pion's momentum is carried either by the quark or the antiquark. However, this is contradicted by the result for $\langle \xi^2 \rangle_2$, calculated from R_2 (as defined in Eq. 5.16), that describes a wavefunction in which the momentum is shared equally between valence quarks.

Combining these results with the definition of the pion's distribution amplitude (Eq. 1.39),

$$\phi_\pi(x, \mu^2) = 6x(1-x) \sum_{n \geq 0} a_n(\mu) C_n^{\frac{3}{2}}(2x-1), \quad (6.1)$$

where $a_0 = 1$ and $a_2(\mu) = 35/12(\langle \xi^2 \rangle(\mu) - 1/5)$, we obtain an expression for $\phi_\pi(x)$. The series in Eq. 6.1 is truncated at $n = 2$. In approximating ϕ_π , we have assumed that the scale is sufficiently high such that contributions to the wavefunction from higher twist terms are negligible. The wavefunctions generated from each value of $\langle \xi^2 \rangle$ are plotted in Fig. 6.1, along with the asymptotic form (for which $\langle \xi^2 \rangle = 1/5$).

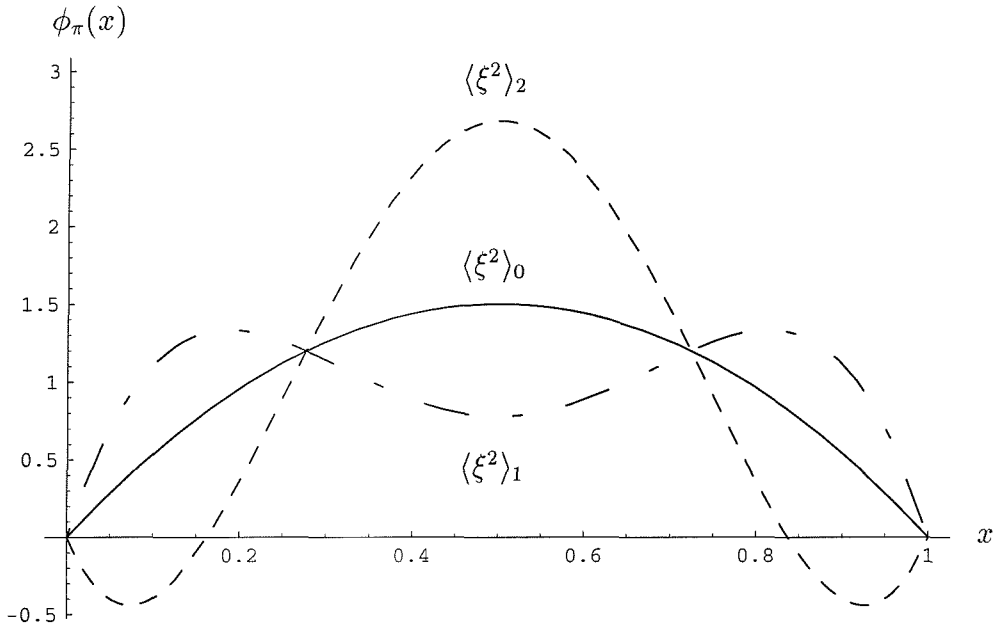


Figure 6.1: The pion's distribution amplitude for $\langle \xi^2 \rangle_0 = 1/5$ (asymptotic form), $\langle \xi^2 \rangle_1 = 0.280$ and $\langle \xi^2 \rangle_2 = 0.021$.

In order to make a comparison with other studies (both in the lattice regularisation scheme and in the $\overline{\text{MS}}$ scheme), the results must be compared at the same scale. All of the lattice studies conducted previously present the results in the lattice regularisation scheme at different scales and therefore we have used quenched¹ one-loop running [63] to obtain results at our lattice scale (2.67 GeV). These are then compared with our bare lattice results. From Table 6.1, we observe that $\langle \xi^2 \rangle_{L_1}$ actually agrees with the previous predictions for the operator corresponding to $\langle \xi^2 \rangle_{L_2}$ [5, 6, 8], originally obtained with inverse lattice spacing $a^{-1} = 1.01$ GeV, $a^{-1} = 1.8$ GeV and $a^{-1} = 1.9$ GeV respectively. The operator corresponding to $\langle \xi^2 \rangle_{L_1}$ was also calculated previously on the lattice [9], however, we do not find agreement with this result. The result for $\langle \xi^2 \rangle_{L_2}$ is well below all values previously predicted for this operator ($O_{\sigma\mu\mu}$) using the lattice.

The comparison with predictions from QCD sum rules (0.4 ± 0.2 at $Q = 1.22$ GeV [10], and 0.39 at $Q = 1.5$ GeV [11]), is made after running the sum rule results in the $\overline{\text{MS}}$ scheme at two loops [63] with the appropriate number of active flavours, up to our lattice scale. From Table 6.1, we see that $\langle \xi^2 \rangle_1$ is in good agreement with sum rule predictions. However, in the case of $\langle \xi^2 \rangle_2$, this is again much smaller.

In summary, we note that the operator used to compute $\langle \xi^2 \rangle_{L_1}$ ($O_{\sigma\{\mu\nu\}}$) agrees with previous values associated with the operator $O_{\sigma\mu\mu}$. When this is matched to the $\overline{\text{MS}}$ scheme, we find satisfactory agreement with sum rule predictions. However, the result for $\langle \xi^2 \rangle_{L_2}$ is incompatible with preceding lattice values for this operator. Furthermore, it is smaller than that of the asymptotic value which is unexpected at this scale. At this stage however, there is no reason to reject the result obtained for the second moment from R_2 and therefore further investigation is necessary.

¹Although the result quoted in reference [9] is calculated using two flavours of sea-quarks, the sea-quark masses are quite heavy.

current results	previous lattice results	QCD sum rules
$\langle \xi^2 \rangle_1 = 0.280(49)^{+30}_{-13}$	$\langle \xi^2 \rangle_{L_2} = 0.235(25)$ [5]	$0.353(61)$ [10]
$\langle \xi^2 \rangle_{L_1} = 0.185(32)$	$\langle \xi^2 \rangle_{L_2} = 0.26(13)$ [6]	
$\langle \xi^2 \rangle_2 = 0.021(8)^{+3}_{-7}$	$\langle \xi^2 \rangle_{L_2} = 0.30(13)$ [8]	0.358 [11]
$\langle \xi^2 \rangle_{L_2} = 0.045(17)$	$\langle \xi^2 \rangle_{L_1} = 0.11(2)$ [9]	
	$\langle \xi^2 \rangle_{L_2} = 0.101(10)$ [9]	

Table 6.1: A comparison between the values of $\langle \xi^2 \rangle$ obtained in this study, previous lattice results (all obtained in the lattice regularisation scheme) and QCD sum rules. The errors on $\langle \xi^2 \rangle_{L_{1,2}}$ are statistical only.

In general, there are a number of ways in which to reduce the error that accompanies the prediction of $\langle \xi^2 \rangle$ using lattice QCD. The most significant source of uncertainty is expected to come from the perturbative renormalisation of the lattice operators. As discussed in Chapter 5, this could be reduced considerably by matching non-perturbatively. The systematic error resulting from $O(a)$ terms could be removed by using improved operators (in addition to the improved action), such that the leading discretisation error is of $O(a^2)$. The statistical error could be reduced by increasing the number of configurations on which the correlators are measured. In addition, the uncertainty introduced by working in the quenched approximation could be avoided by simulating the operators using dynamical fermions.

Possible phenomenological extensions of this study include an analysis of the fourth and sixth moments of the distribution amplitude. However, this would undoubtedly require a non-perturbative computation of the matching coefficients due to the increased number of derivatives in the operators. Furthermore, contributions to the shape of the distribution amplitude from higher twist terms are expected to be small at higher energies. Another possibility would be to perform a similar analysis of particles such as the ρ -meson and the kaon. This would

provide valuable non-perturbative information necessary to describe other decay modes of B mesons [18]. We also note that the lowest moments of baryon distribution amplitudes are useful in order to compute the proton's electromagnetic form factor. This is particularly interesting since experiment currently disagrees with the theoretical predictions of the asymptotic form of the proton wavefunction.

Bibliography

- [1] G. R. Farrar and D. R. Jackson, Phys. Rev. Lett. **43**, 246 (1979).
- [2] G. P. Lepage and S. J. Brodsky, Phys. Rev. **D22**, 2157 (1980).
- [3] A. V. Efremov and A. V. Radyushkin, Theor. Math. Phys. **42**, 97 (1980).
- [4] S. J. Brodsky and G. P. Lepage, Adv. Ser. Direct. High Energy Phys. **5**, 149 (1989).
- [5] S. Gottlieb and A. S. Kronfeld, Phys. Rev. **D33**, 227 (1986).
- [6] G. Martinelli and C. T. Sachrajda, Phys. Lett. **B190**, 151 (1987).
- [7] G. Martinelli and C. T. Sachrajda, Nucl. Phys. **B306**, 865 (1988).
- [8] T. A. DeGrand and R. D. Loft, Phys. Rev. **D38**, 954 (1988).
- [9] D. Daniel, R. Gupta, and D. G. Richards, Phys. Rev. **D43**, 3715 (1991).
- [10] V. L. Chernyak and A. R. Zhitnitsky, Phys. Rept. **112**, 173 (1984).
- [11] M. J. Lavelle, Zeit. Phys. **C29**, 203 (1985).
- [12] P. Ball and V. M. Braun, Phys. Rev. **D54**, 2182 (1996).
- [13] P. Ball, V. M. Braun, Y. Koike, and K. Tanaka, Nucl. Phys. **B529**, 323 (1998).

- [14] P. Ball, JHEP **01**, 010 (1999).
- [15] G. Sterman and P. Stoler, Hadronic form factors and perturbative QCD, 1997, hep-ph/9708370.
- [16] A. V. Efremov and A. V. Radyushkin, Phys. Lett. **B94**, 245 (1980).
- [17] V. Savinov, A Measurement of the form-factors of light pseudoscalar mesons at a large momentum transfer, 1995, hep-ex/9507005.
- [18] M. Beneke, G. Buchalla, M. Neubert, and C. T. Sachrajda, Nucl. Phys. **B591**, 313 (2000).
- [19] M. Beneke, G. Buchalla, M. Neubert, and C. T. Sachrajda, Nucl. Phys. **B606**, 245 (2001).
- [20] T. Iijima, Study of rare B meson decays at Belle, 2001, hep-ex/0105005.
- [21] J. Beringer, CP violation, B mixing and B lifetime results from the BaBar experiment, 2001, hep-ex/0105073.
- [22] S. J. Brodsky, Y. Frishman, G. P. Lepage, and C. Sachrajda, Phys. Lett. **B91**, 239 (1980).
- [23] D. Muller, Phys. Rev. **D51**, 3855 (1995).
- [24] V. L. Chernyak and A. R. Zhitnitsky, Nucl. Phys. **B201**, 492 (1982).
- [25] D. A. Johnston and H. F. Jones, Z. Phys. **C33**, 281 (1986).
- [26] M. A. Shifman, A. I. Vainshtein, and V. I. Zakharov, Nucl. Phys. **B147**, 385 (1979).
- [27] L. Lellouch and M. Luscher, Commun. Math. Phys. **219**, 31 (2001).
- [28] P. Boucaud *et al.*, Extraction of K to pi pi matrix elements with Wilson fermions, 2001, hep-lat/0110169.

[29] P. Boucaud *et al.*, K to pi pi matrix elements beyond the leading-order chiral expansion, 2001, hep-lat/0110206.

[30] K. G. Wilson, Phys. Rev. **D10**, 2445 (1974).

[31] M. Creutz, Quarks, Gluons and Lattices; Cambridge University Press, Cambridge, 1983.

[32] K. Rothe, Lattice Gauge Theories An Introduction; World Scientific Publishing Company 1997.

[33] I. Montvay and G. Munster, Quantum fields on a Lattice; Cambridge University Press 1994.

[34] R. Gupta, Introduction to lattice QCD, 1997, arXiv:hep-lat/9807028.

[35] S. R. Sharpe, Phenomenology from the lattice, 1994, arXiv:hep-ph/9412243.

[36] C. T. Sachrajda, LATTICE PERTURBATION THEORY, lectures given at Theoretical Adv. Study Inst. in Elementary Particle Physics, Boulder, CO, Jun 4-30, 1989.

[37] Nielsen, Holger Bech and Ninomiya, M, Phys. Lett. **B105**, 219 (1981).

[38] L. H. Karsten and J. Smit, Nucl. Phys. **B183**, 103 (1981).

[39] A. Gonzalez Arroyo, F. J. Yndurain, and G. Martinelli, Phys. Lett. **B117**, 437 (1982).

[40] P. H. Ginsparg and K. G. Wilson, Phys. Rev. **D25**, 2649 (1982).

[41] P. Hernandez, K. Jansen, and M. Luscher, Nucl. Phys. **B552**, 363 (1999).

[42] B. Efron, The Jackknife, the Bootstrap and other Resampling Plans; (Soc. for Industrial and Applied mathematics).

[43] K. Symanzik, Nucl. Phys. **B226**, 187 (1983).

- [44] B. Sheikholeslami and R. Wohlert, Nucl. Phys. **B259**, 572 (1985).
- [45] G. Heatlie *et al.*, Nucl. Phys. **B352**, 266 (1991).
- [46] M. Luscher, S. Sint, R. Sommer, and P. Weisz, Nucl. Phys. **B478**, 365 (1996).
- [47] A. S. Kronfeld and D. M. Photiadis, Phys. Rev. **D31**, 2939 (1985).
- [48] H. F. Jones, Groups, Representations and Physics; Institute of Physics Publishing 1990.
- [49] D. Olive, Group theory lectures, University of Wales, Swansea, 1998.
- [50] J. E. Mandula, G. Zweig, and J. Govaerts, Nucl. Phys. **B228**, 91 (1983).
- [51] G. Martinelli *et al.*, Nucl. Phys. **B445**, 81 (1995).
- [52] M. Gockeler *et al.*, Nucl. Phys. **B472**, 309 (1996).
- [53] G. P. Lepage and P. B. Mackenzie, Phys. Rev. **D48**, 2250 (1993).
- [54] A. Billoire, Phys. Lett. **B104**, 472 (1981).
- [55] W. Fischler, Nucl. Phys. **B129**, 157 (1977).
- [56] M. Luscher and P. Weisz, Nucl. Phys. **B452**, 234 (1995).
- [57] K. C. Bowler *et al.*, Phys. Rev. **D62**, 054506 (2000).
- [58] M. Guagnelli, R. Sommer, and H. Wittig, Nucl. Phys. **B535**, 389 (1998).
- [59] M. Creutz, Phys. Rev. **D36**, 515 (1987).
- [60] F. R. Brown and T. J. Woch, Phys. Rev. Lett. **58**, 2394 (1987).
- [61] N. Cabibbo and E. Marinari, Phys. Lett. **B119**, 387 (1982).
- [62] S. Pickles, PhD thesis, University of Edinburgh, 1998.

- [63] B. Melic, B. Nizic, and K. Passek, Phys. Rev. **D60**, 074004 (1999).
- [64] M. R. Spiegel, Probability and Statistics; Schaum's Outlines, McGraw-Hill, 1998.
- [65] H. Kawai, R. Nakayama, and K. Seo, Nucl. Phys. **B189**, 40 (1981).

Appendix A

The moments of a distribution

In this section, we introduce the moments of a distribution and demonstrate the way in which they characterise and therefore provide insight into the form of a distribution. The material contained within is based on Ref. [64]. In order to illustrate the ideas and definitions clearly, we begin with a brief introduction to the expectation, variance and standard deviation of a distribution.

A.1 Expectation

The definition of expectation for a *discrete* random variable X with possible values x_1, x_2, \dots, x_n is defined as

$$E(X) = \sum_{j=1}^n x_j f(x_j), \quad (\text{A.1})$$

where $f(x_j)$ is the probability that $X = x_j$. For a *continuous* random variable X

with density function $f(x)$, the expectation of X is defined as

$$E(X) = \int_{-\infty}^{\infty} xf(x)dx. \quad (\text{A.2})$$

The expectation of X is usually called the mean μ . This single value represents the average of X and is therefore considered as a measure of the central tendency of the distribution of X .

A.2 The variance and standard deviation

Having defined the mean μ as the expectation of a random variable in Eq. A.1 and Eq. A.2 for the discrete and continuous case respectively, we now introduce another important quantity called the variance which is defined by

$$V(X) = E[(X - \mu)^2], \quad (\text{A.3})$$

which is a positive quantity also denoted as σ^2 . Explicitly, if X is a *discrete* random variable with probability function $f(x)$, then the variance is given by

$$\sigma^2 = \sum (x - \mu)^2 f(x). \quad (\text{A.4})$$

In the case of a *continuous* random variable with density function $f(x)$, the variance is defined to be

$$\sigma^2 = \int_{-\infty}^{\infty} (x - \mu)^2 f(x) dx. \quad (\text{A.5})$$

The standard deviation is obtained by taking the positive square root of Eq. A.3, i.e.

$$\sigma = \sqrt{V(X)} = \sqrt{E[(x - \mu)^2]}. \quad (\text{A.6})$$

Both the variance and the standard deviation are a measure of the dispersion of the values of the random variable about the mean μ . Another way to say this is that they provide insight into the shape of $f(x)$, the probability distribution (for the discrete case) or the density function (continuous case). For values that are concentrated around μ , the variance is small and the density function has a peaked shape. Conversely, if the values are scattered with many distributed far from the mean, the variance is large and the density function has a flatter appearance. These distributions are illustrated in Fig. A.1 below.

A.3 The moments of a distribution

Following on from the variance, we can now generalise to the moments of a random variable X , which characterise the form of the distribution $f(x)$ about the mean. Explicitly, the n^{th} moment about the mean μ is defined as

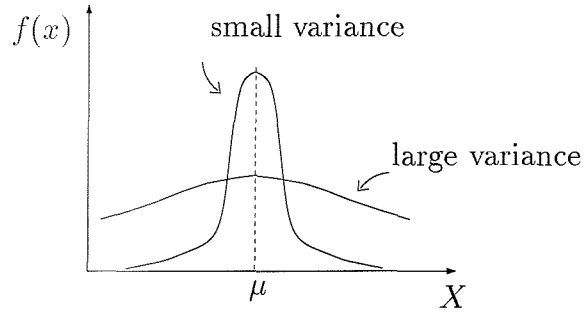


Figure A.1: Density functions with small and large variance.

$$\langle \xi^n \rangle = E[(X - \mu)^n], \quad (\text{A.7})$$

where $n = 0, 1, \dots$. From Eq. A.7, it can be seen that the zeroth moment $\xi^0 = 1$, the first moment $\xi^1 = 0$ and the second moment $\xi^2 = E[(X - \mu)^2]$ which (from Eq. A.3) is the variance. Since this study focuses on the second moment, we do not consider the higher moments.

Since we are interested in the second moment of the pion's distribution amplitude where $\phi(\xi)$ is a continuous distribution, we state the equation for the moments of a continuous distribution about the mean

$$\langle \xi^n \rangle = \int_{-\infty}^{\infty} (\xi - \mu)^n f(\xi) d\xi. \quad (\text{A.8})$$

For a distribution with mean $\mu = 0$, the n^{th} moment is defined as

$$\xi_n = \int_{-\infty}^{\infty} \xi^n f(\xi) dx. \quad (\text{A.9})$$

To relate this to the main text, we note the following points.

- $\xi = u - \bar{u}$ where u and \bar{u} are the fractions of momentum carried by the quark and antiquark
- the limits in Eq. A.8 are $[-1, 1]$ since the fraction of momentum ranges between zero and one.
- $\phi(\xi)$ is symmetric i.e. $\phi(\xi) = \phi(-\xi)$

Appendix B

Group theory

In this section, we present the character tables for the operators of interest.

B.1 The hypercubic group

Table B.1 displays a typical element of the hypercubic group (\mathcal{H}_4) for each conjugacy class. The characters for the irreducible representations of \mathcal{H}_4 can be found in Tables 5.2a-c, Ref. [50].

B.2 Obtaining the characters for each representation

Since we do not know the matrix form of the representation, we take an element from a particular class and act on the operators which form a basis. For example, consider the component $p_1 q_2 r_3$ of $O_{\sigma\mu\nu}$ under the reflection of both the 1- and

class	order	no. of elts.	typical element
			permutation/reflection notation
A	1	1	I
B	2	6	$P_1 P_2$
C	2	1	$P_1 P_2 P_3 P_4$
D	4	12	$(12)P_1$
E	2	24	$(12)P_3$
F	4	12	$(12)P_1 P_3 P_4$
G	3	32	(123)
H	6	32	$(123)P_1 P_4$
I	8	24	$(1234)P_1$
J	2	12	$(12)(34)$
K	4	12	$(12)(34)P_1 P_2$
L	2	4	$(-1)P_1$
M	2	4	$(-1)P_1 P_2 P_3$
N	2	12	$(-1)(12)$
O	4	24	$(-1)(12)P_1 P_3$
P	2	12	$(-1)(12)P_3 P_4$
Q	6	32	$(-1)(123)P_1$
R	6	32	$(-1)(123)P_4$
S	4	48	$(-1)(1234)$
T	4	24	$(-1)(12)(34)P_1$

Table B.1: Typical element for each conjugacy class of the hypercubic group

2-axis.

$$\begin{aligned}
 p_1 q_2 r_3 &\xrightarrow{P_1 P_2} (-p_1)(-q_2)r_3 \\
 &= p_1 q_2 r_3
 \end{aligned}$$

Since the component is invariant under this operation, this implies that there is an entry of 1 along the diagonal of the representation. If however we consider a permutation of the indices of $O_{\sigma\mu\nu}$, since all indices are different, this implies a zero entry for the diagonal element of the representation.

To summarise,

- component left unchanged: enter +1
- for an odd number of reflections: enter -1
- for a permutation of the axes for $O_{\sigma\mu\nu}$: enter 0
- for a permutation of the 2- and 3-axes for $O_{\sigma\mu\mu}$: enter 1

Following this simple set of rules, Tables B.2 - B.6 are completed.

Note that the components in Table B.6 are defined as

$$\begin{aligned} F(p_\sigma, q_\mu, r_\nu) = & \frac{1}{2} [p_\sigma q_\mu r_\nu + p_\sigma q_\nu r_\mu \\ & + p_\nu q_\sigma r_\mu + p_\nu q_\mu r_\sigma - 2p_\mu q_\nu r_\sigma - 2p_\mu q_\sigma r_\nu] \end{aligned} \quad (\text{B.1})$$

and

$$G(p_\sigma, q_\mu, r_\nu) = \frac{1}{2\sqrt{3}} [p_\sigma q_\mu r_\nu + p_\sigma q_\nu r_\mu - p_\nu q_\sigma r_\mu - p_\nu q_\mu r_\sigma]. \quad (\text{B.2})$$

basis components	class and typical element						
	A	B	C	D-K	L	M	N-T
$p_\sigma q_\mu r_\nu$	I	$P_1 P_2$	$P_1 P_2 P_3 P_4$	-	P_1	$P_1 P_2 P_3$	-
$p_1 q_2 r_3$	1	1	-1	0	1	1	0
$p_1 q_2 r_4$	1	1	-1	0	1	-1	0
$p_1 q_3 r_2$	1	1	-1	0	1	1	0
$p_1 q_3 r_4$	1	-1	-1	0	1	-1	0
$p_1 q_4 r_2$	1	1	-1	0	1	-1	0
$p_1 q_4 r_3$	1	-1	-1	0	1	-1	0
$p_2 q_1 r_3$	1	1	-1	0	1	1	0
$p_2 q_1 r_4$	1	1	-1	0	1	-1	0
$p_2 q_3 r_1$	1	1	-1	0	1	1	0
$p_2 q_3 r_4$	1	-1	-1	0	-1	-1	0
$p_2 q_4 r_1$	1	1	-1	0	1	-1	0
$p_2 q_4 r_3$	1	-1	-1	0	-1	-1	0
$p_3 q_1 r_2$	1	1	-1	0	1	1	0
$p_3 q_1 r_4$	1	-1	-1	0	1	-1	0
$p_3 q_2 r_1$	1	1	-1	0	1	1	0
$p_3 q_2 r_4$	1	-1	-1	0	-1	-1	0
$p_3 q_4 r_1$	1	-1	-1	0	1	-1	0
$p_3 q_4 r_2$	1	-1	-1	0	-1	-1	0
$p_4 q_1 r_2$	1	1	-1	0	1	-1	0
$p_4 q_1 r_3$	1	-1	-1	0	1	-1	0
$p_4 q_2 r_1$	1	1	-1	0	1	-1	0
$p_4 q_2 r_3$	1	-1	-1	0	-1	-1	0
$p_4 q_3 r_1$	1	-1	-1	0	1	-1	0
$p_4 q_3 r_2$	1	-1	-1	0	-1	-1	0
$Tr[R(g)]$	24	0	-24	0	12	-12	0

Table B.2: Characters of the 24 dimensional representation $O_{\sigma\mu\nu}$

basis components	class												
	A	B	C	D	E	F	G-K	L	M	N	O	P	Q-T
$p_1 q_2^2$	1	-1	-1	0	0	0	0	1	1	0	0	0	0
$p_1 q_3^2$	1	-1	-1	0	0	0	0	1	1	0	0	0	0
$p_1 q_4^2$	1	-1	-1	0	0	0	0	1	1	0	0	0	0
$p_2 q_1^2$	1	-1	-1	0	0	0	0	-1	1	0	0	0	0
$p_2 q_3^2$	1	-1	-1	0	0	0	0	-1	1	0	0	0	0
$p_2 q_4^2$	1	-1	-1	0	0	0	0	-1	1	0	0	0	0
$p_3 q_1^2$	1	1	-1	0	0	0	0	-1	1	0	0	0	0
$p_3 q_2^2$	1	1	-1	0	0	0	0	-1	1	0	0	0	0
$p_3 q_4^2$	1	1	-1	1	-1	-1	0	-1	1	-1	1	1	0
$p_4 q_1^2$	1	1	-1	0	0	0	0	-1	-1	0	0	0	0
$p_4 q_2^2$	1	1	-1	0	0	0	0	-1	-1	0	0	0	0
$p_4 q_3^2$	1	1	-1	1	1	-1	0	-1	-1	-1	-1	1	0
$Tr[R(g)]$	12	0	-12	2	0	-2	0	-6	6	-2	0	2	0

Table B.3: Characters of the 12 dimensional representation $O_{\sigma\mu\mu}$

basis components	class												
	A	B	C	D	E	F	G-K	L	M	N	O	P	Q-T
$p_1 q_2 r_3$	1	1	-1	0	0	0	0	1	1	0	0	0	0
$p_1 q_2 r_4$	1	1	-1	0	0	0	0	1	-1	0	0	0	0
$p_1 q_3 r_4$	1	-1	-1	0	0	0	0	1	-1	0	0	0	0
$p_2 q_1 r_3$	1	1	-1	0	0	0	0	1	1	0	0	0	0
$p_2 q_1 r_4$	1	1	-1	0	0	0	0	1	-1	0	0	0	0
$p_2 q_3 r_4$	1	-1	-1	0	0	0	0	-1	-1	0	0	0	0
$p_3 q_1 r_2$	1	1	-1	-1	-1	1	0	1	1	-1	-1	1	0
$p_3 q_1 r_4$	1	-1	-1	0	0	0	0	1	-1	0	0	0	0
$p_3 q_2 r_4$	1	-1	-1	0	0	0	0	-1	-1	0	0	0	0
$p_4 q_1 r_2$	1	1	-1	-1	1	1	0	1	1	-1	1	1	0
$p_4 q_1 r_3$	1	-1	-1	0	0	0	0	1	-1	0	0	0	0
$p_4 q_2 r_3$	1	-1	-1	0	0	0	0	-1	-1	0	0	0	0
$Tr[R(g)]$	12	0	-12	-2	0	2	0	6	-6	-2	0	2	0

Table B.4: Characters of the 12 dimensional representation $O_{\sigma\{\mu\nu\}}$ where μ and ν are symmetrised

basis components	class												
	A	B	C	D-F	G	H	I-K	L	M	N-P	Q	R	S-T
$p_4[p_1^2 - \frac{p_2^2+p_3^2}{2}]$	1	1	-1	0	0	0	0	-1	-1	0	0	0	0
$p_4[p_2^2 - \frac{p_1^2+p_3^2}{2}]$	1	1	-1	0	-1	1	0	-1	-1	0	1	-1	0
$p_3[p_1^2 - \frac{p_2^2+p_4^2}{2}]$	1	1	-1	0	0	0	0	-1	1	0	0	0	0
$p_3[p_1^2 - \frac{p_1^2+p_2^2}{2}]$	1	1	-1	0	0	0	0	-1	1	0	0	0	0
$p_2[p_1^2 - \frac{p_3^2+p_4^2}{2}]$	1	-1	-1	0	0	0	0	-1	1	0	0	0	0
$p_2[p_3^2 - \frac{p_1^2+p_4^2}{2}]$	1	-1	-1	0	0	0	0	-1	1	0	0	0	0
$p_1[p_2^2 - \frac{p_3^2+p_4^2}{2}]$	1	-1	-1	0	0	0	0	1	1	0	0	0	0
$p_1[p_3^2 - \frac{p_2^2+p_4^2}{2}]$	1	-1	-1	0	0	0	0	1	1	0	0	0	0
$Tr[R(g)]$	8	0	-8	0	-1	1	0	-4	4	0	1	-1	0

Table B.5: Characters of the $\mathbf{8}^{(-)}$ dimensional representation

basis components	class												
	A	B	C	D-F	G	H	I-K	L	M	N-P	Q	R	S-T
$F(p_1, q_2, r_3)$	1	1	-1	0	-1	1	0	1	1	0	-1	1	0
$F(p_1, q_2, r_4)$	1	1	-1	0	0	0	0	1	-1	0	0	0	0
$F(p_1, q_3, r_4)$	1	-1	-1	0	0	0	0	1	-1	0	0	0	0
$F(p_2, q_3, r_4)$	1	-1	-1	0	0	0	0	-1	-1	0	0	0	0
$G(p_1, q_2, r_3)$	1	1	-1	0	-1	1	0	1	1	0	-1	1	0
$G(p_1, q_2, r_4)$	1	1	-1	0	0	0	0	1	-1	0	0	0	0
$G(p_1, q_3, r_4)$	1	-1	-1	0	0	0	0	1	-1	0	0	0	0
$G(p_2, q_3, r_4)$	1	-1	-1	0	0	0	0	-1	-1	0	0	0	0
$Tr[R(g)]$	8	0	-8	0	-2	2	0	4	-4	0	-2	2	0

Table B.6: Characters of the $\mathbf{8}^{(+)}$ dimensional representation

Appendix C

Feynman diagrams

In this section, the Feynman rules in both the continuum and lattice [65] regularisation schemes are presented. In Sec. C.2, we illustrate the one-loop diagrams necessary to compute the matching coefficients for the operators of interest. In Sec. C.3, we outline the calculation of the sail diagrams on the lattice.

We note that in Sec. C.1.2, the following notation is used

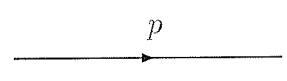
$$\Gamma = \gamma_\sigma \gamma_5, \quad (C.1)$$

$$\bar{p}_\mu = \frac{2}{a} \sin(ap_\mu), \quad (C.2)$$

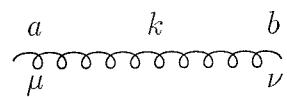
where a is the lattice spacing.

C.1 Feynman rules

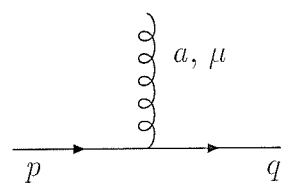
C.1.1 Continuum Feynman rules (Minkowski space)



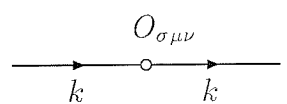
$$D(p) = \frac{i(p+m)}{p^2 - m^2}$$



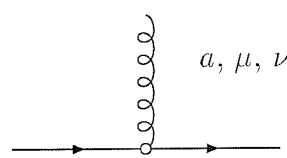
$$G_{ab}^{\mu\nu}(p) = \frac{-i\delta_{ab}\delta^{\mu\nu}}{(k^2 - \lambda^2)}$$



$$V_\mu(p, q) = -ig\gamma^\mu t^a$$

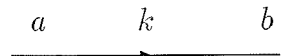


$$O_F = -4\Gamma k_\mu k_\nu t^a$$

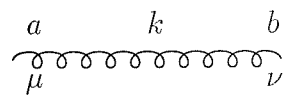


$$O_{FG} = -4g\Gamma [k_\mu A_\nu^a + k_\nu A_\mu^a] t^a$$

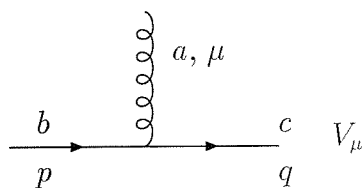
C.1.2 Lattice Feynman rules (Euclidean space)



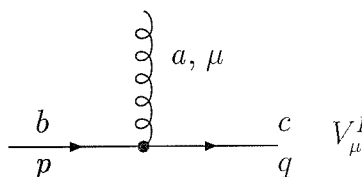
$$D(k) = \frac{\delta_{\mu\nu}}{\frac{1}{a} \sum_{\alpha} i \gamma_{\alpha} \sin(ak_{\alpha}) + \frac{r}{2} k^2}$$



$$G_{\mu\nu} = \frac{\delta_{ab} \delta_{\mu\nu}}{k^2 - a^2 \lambda^2}$$

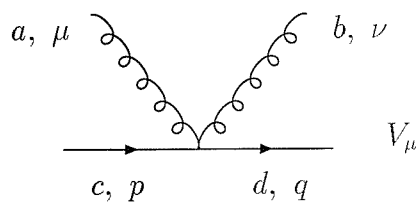


$$V_{\mu}(p, q) = -ig \left[\gamma_{\mu} \cos\left(\frac{ap+aq}{2}\right)_{\mu} - \frac{i}{2} r(\overline{p+q})_{\mu} \right] (t^a)_{bc}$$

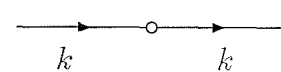


$$V_{\mu}^I(p, q) = g c_{SW} \frac{r}{2} \left[\sum_{\nu} \sigma_{\rho\nu} \sin(ap - aq)_{\nu} \cos\left(\frac{ap-aq}{2}\right)_{\rho} \right] (t^a)_{bc}$$

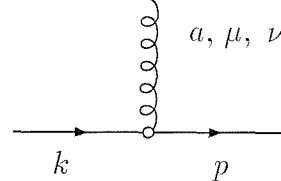
$$\text{where } \sigma_{\rho\nu} = \frac{1}{2} [\gamma_{\rho}, \gamma_{\nu}]$$



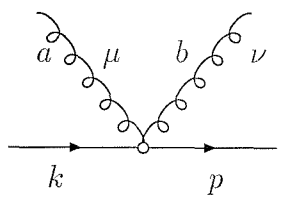
$$V_{\mu\nu}(p, q) = -\frac{aq^2}{2} \delta_{\mu\nu} \left[r \cos\left(\frac{ap+aq}{2}\right)_{\mu} - \frac{ia}{2} \gamma_{\mu} (\overline{ap+aq})_{\mu} \right] \{t^a, t^b\}_{cd}$$



$$O_F = -4g\Gamma \sin(ak_\mu) \sin(ak_\nu)$$



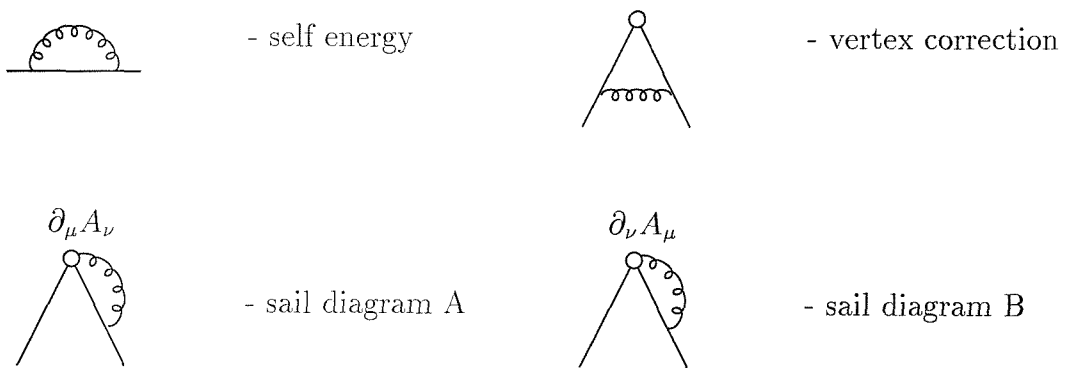
$$O_{FG} = -4\frac{g}{a}\Gamma [\sin(ak_\mu) \cos(\frac{(p+k)_\nu}{2}) + \sin(ap_\nu) \cos(\frac{(p+k)_\mu}{2})](t^a)_{bc}$$



$$O_{FGG} = 2\Gamma \sin(ap_\nu) \sin(\frac{k+p}{2})_\mu t^a t^b + 2\Gamma \sin(ap_\mu) \sin(\frac{k+p}{2})_\nu t^a t^b - 4\Gamma \cos(p - \frac{k}{2})_\mu \cos(p + \frac{k'}{2})_\nu t^a t^b$$

C.2 One-loop contributions

Continuum Feynman diagrams ($\circ = O_{\sigma\mu\nu}$):

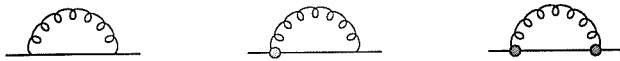


Lattice Feynman diagrams

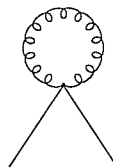
$\circ = O_{\sigma\mu\nu}; O_{\sigma\mu\mu}$

$\bullet = \text{clover improved vertex}$

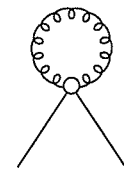
self energy:



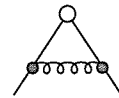
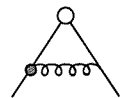
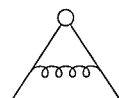
tadpole correction:



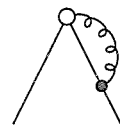
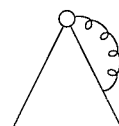
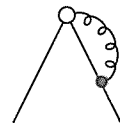
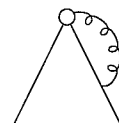
$O_{\sigma\mu\mu}$ tadpole correction:



vertex correction:



sail diagrams:



C.3 An example Feynman diagram on the lattice

In order to demonstrate how Feynman diagrams are computed on the lattice, we outline the steps involved in calculating the sail diagrams for the operator $O_{\sigma\mu\nu}$ (see Sec. C.2 and note that we do not include the clover improved vertex in this example). Before computing the diagrams, we make the following definitions:

$$s_\mu = \sin(ak_\mu), \quad (C.3)$$

$$c_\mu = \cos(ak_\mu), \quad (C.4)$$

$$s_\mu \left(\frac{k}{2} \right) = \sin \left(\frac{ak_\mu}{2} \right), \quad (C.5)$$

$$c_\mu \left(\frac{k}{2} \right) = \cos \left(\frac{ak_\mu}{2} \right), \quad (C.6)$$

$$\Delta_1 = \sum_\alpha \sin^2 \left(\frac{ak_\alpha}{2} \right), \quad (C.7)$$

$$\text{and} \quad \hat{k} = \frac{2}{a} \sin \left(\frac{ak_\mu}{2} \right), \quad (C.8)$$

where a is the lattice spacing.

The sail diagram is written as

$$I = \int_{-\frac{\pi}{2}}^{\frac{\pi}{2}} \frac{d^4 k}{(2\pi)^4} V_\mu(p, q) D(k) O_{FG} G_{\mu\nu}, \quad (C.9)$$

and inserting the Feynman rules, this expression can be split into two contributions, labelled S_a and S_b , each corresponding to a term in O_{FG} . Performing a Taylor expansion around $ap_\mu = 0$ so that we can pick out terms that have the

correct continuum behaviour, we obtain

$$\begin{aligned}
S_a = ig^2 C_F \int \frac{d^4 k}{(2\pi)^4} & \left[\gamma_\nu c_\nu \left(\frac{k}{2} \right) - ir s_\nu \left(\frac{k}{2} \right) - \frac{ap_\nu}{2} \left[\gamma_\nu s_\nu \left(\frac{k}{2} \right) + ir c_\nu \left(\frac{k}{2} \right) \right] \right. \\
& \left. + \frac{a^2 p_\nu^2}{8} \left[-\gamma_\nu c_\nu \left(\frac{k}{2} \right) + ir s_\nu \left(\frac{k}{2} \right) \right] \right] \frac{1}{G_q(k)} [-i\gamma_\alpha s_\alpha + 2r\Delta_1] \\
& \Gamma \left[s_\mu c_\nu \left(\frac{k}{2} \right) - \frac{ap_\nu}{2} s_\mu s_\nu \left(\frac{k}{2} \right) - \frac{a^2 p_\nu^2}{8} s_\mu c_\nu \left(\frac{k}{2} \right) \right] \\
\sum_\lambda & \frac{a^2}{G_g(k)} \left[1 + \frac{ap_\lambda}{2G_g(k)} s_\lambda - \frac{a^2 p_\lambda^2}{4G_g(k)} c_\lambda + \frac{a^2 p_\lambda p_\rho}{4G_g(k)^2} s_\lambda s_\rho \right], \quad (C.10)
\end{aligned}$$

where the colour factor $C_F = 4/3$, $\Gamma = \gamma_\sigma \gamma_5$ and $G(k)$ is the denominator of the quark propagator given by

$$G_q(k) = s^2 + 4r^2 \Delta_1^2 \quad (C.11)$$

The gluon propagator in Eq. C.10 has the denominator

$$G_g(k) = \sum_\alpha s_\alpha^2 \left(\frac{ak}{2} \right) + \frac{a^2 \lambda^2}{4}, \quad (C.12)$$

where λ is the gluon mass introduced to regulate the IR divergence.

Terms with an odd number of sin functions will vanish in Eq. C.10 and terms which are of lower order than $O(a^2 p_\mu^2)$ cancel. Commuting the gamma matrices to the right produces terms which are proportional to $p^2 g_{\mu\nu} \Gamma$ and $p_\mu \gamma_\nu \Gamma$, both of which can be removed since p^2 is small and the latter is proportional to m_q (from the Equations of Motion). Eq. C.10 thus reduces to

$$S_a = g^2 C_F p_\mu p_\nu \Gamma \int \frac{d^4 k}{(2\pi)^4} \frac{a^4}{4G_q(k)} \left[\frac{1}{G_g(k)^3} \left[4s_\mu^2 s_\nu^2 - 2s_\mu^2 s_\nu^2 s_\nu^2 \left(\frac{k}{2} \right) \right] \right]$$

$$\begin{aligned}
& -2s_\mu^2 s_\sigma^2 s_\nu^2 \left(\frac{k}{2} \right) + 2r^2 \Delta_1 s_\mu^2 s_\nu^2 \Big] \\
& + \frac{1}{G_g(k)^2} \left[-\frac{1}{2} s_\mu^2 s_\nu^2 - 2r^2 \Delta_1 s_\mu^2 s_\nu^2 \left(\frac{k}{2} \right) \right] \\
& + \frac{1}{G_g(k)} \left[-\frac{1}{2} s_\mu^2 s_\nu^2 + 2r^2 \Delta_1 s_\mu^2 c_\nu^2 \left(\frac{k}{2} \right) \right] \Big], \quad (\text{C.13})
\end{aligned}$$

where we note that by power counting, the first term is IR divergent. Before dealing with this divergence and the additional finite terms, we write down the expression for the second term in Eq. C.9,

$$\begin{aligned}
S_b = ig^2 C_F \int \frac{d^4 k}{(2\pi)^4} & \left[\gamma_\nu c_\nu \left(\frac{k}{2} \right) - ir s_\nu \left(\frac{k}{2} \right) - \frac{ap_\nu}{2} \left[\gamma_\nu s_\nu \left(\frac{k}{2} \right) + ir c_\nu \left(\frac{k}{2} \right) \right] \right. \\
& \left. + \frac{a^2 p_\nu^2}{8} \left[-\gamma_\nu c_\nu \left(\frac{ak}{2} \right) + ir s_\nu \left(\frac{ak}{2} \right) \right] \right] \\
& \frac{1}{G_q(k)} \left[-i\gamma_\alpha s_\alpha + 2r \Delta_1 \right] \Gamma \left[\frac{ap_\nu}{2} c_\mu \left(\frac{k}{2} \right) - \frac{a^2 p_\mu p_\nu}{2} s_\mu \left(\frac{k}{2} \right) \right] \\
& \sum_\lambda \frac{a^2}{G_g(k)} \left[1 + \frac{ap_\lambda}{2G_g(k)} s_\lambda - \frac{a^2 p_\lambda^2}{4G_g(k)} c_\lambda + \frac{a^2 p_\lambda p_\rho}{4G_g(k)^2} s_\lambda s_\rho \right]. \quad (\text{C.14})
\end{aligned}$$

As with S_a , terms of lower order than $O(a^2 p^2)$ cancel. The gamma matrices in the remaining terms are commuted to the right and neglecting terms proportional to p^2 , Eq. C.14 reduces to

$$\begin{aligned}
S_b = g^2 C_F p_\mu p_\nu \Gamma \int \frac{d^4 k}{(2\pi)^4} \frac{a^4}{2G_q(k)} & \left[\frac{1}{G_g(k)^3} \left[c_\mu^2 \left(\frac{k}{2} \right) (s_\mu^2 + s_\nu^2) + r^2 \Delta_1 s_\nu^2 \right] \right. \\
& \left. + \frac{1}{G_g(k)} \left[-s_\mu^2 + 2r^2 \Delta_1 \left(1 - 2s_\mu^2 \left(\frac{k}{2} \right) \right) \right] \right], \quad (\text{C.15})
\end{aligned}$$

where the first term contains IR divergent terms. Combining S_a and S_b , we obtain

$$S_a + S_b = -4p_\mu p_\nu \Gamma g^2 C_F \int \frac{d^4 k}{(2\pi)^4} \frac{a^4}{G(k)} \left[\frac{A}{G_g(k)^3} + \frac{B}{G_g(k)^2} \right]$$

$$+ \frac{C}{G_g(k)} + \frac{1}{2}s_\mu^2 - \frac{1}{4} \Big] , \quad (C.16)$$

where,

$$A = \underbrace{-4s_\mu^2 s_\nu^2 + 10s_\mu^4 s_\nu^2 - 6s_\mu^4 s_\nu^4 - 2s_\mu^2 s_\nu^6 + 2s_\mu^4 s_\nu^6 + 2s_\mu^2 s_\nu^2 s_\sigma^2}_{- 4s_\mu^4 s_\nu^2 s_\sigma^2 + 2s_\mu^4 s_\nu^4 s_\sigma^2} \quad (C.17)$$

$$B = - \underbrace{s_\mu^2}_{s_\mu^2} - \frac{1}{2}s_\mu^2 s_\nu^2 + \frac{3}{2}s_\mu^2 s_\nu^4 - s_\mu^4 s_\nu^4 + \frac{3}{2}s_\mu^4 - \frac{1}{2}s_\mu^6 \quad (C.18)$$

$$C = s_\mu^2 s_\nu^2 - s_\mu^2 s_\nu^4 - \frac{1}{2}s_\mu^2 + \frac{1}{2}s_\mu^4 \quad (C.19)$$

and terms denoted with an underbrace are IR divergent. These are dealt with by subtracting and adding the divergent part. This leaves a finite term that, with the other finite terms, can be computed numerically and a divergent term which is calculated analytically. The result of the divergent integral is logarithmic, depending on the lattice spacing and the gluon mass (the IR regulator). Explicitly, the overall result for these two diagrams (including the symmetric combinations) is given by

$$2(S_a + S_b) = (-4\Gamma p_\mu p_\nu) \frac{\alpha}{4\pi} C_F \left[\frac{-10}{3} \log \left(\frac{1}{a^2 \lambda^2} \right) - 2.171 \right]. \quad (C.20)$$

The results for all the one-loop diagrams are given in Table 4.1 (continuum), and Table 4.2 (lattice), Ch. 4.